Translational Research 255 (2023) 50–65

Contents lists available at ScienceDirect

Translational Research

journal homepage: www.elsevier.com/locate/jagp

Original Research Article

# The E3 ubiquitin ligase CHIP protects against sepsis-induced myocardial dysfunction by inhibiting NF-κB-mediated inflammation via promoting ubiquitination and degradation of karyopherin-α 2

Jia Liao [1,#], Xingyu Su [1,#], Miao Wang [1], Lucen Jiang [2], Xi Chen [3], Zixi Liu [1], Guoqing Tang [1], Li Zhou [4], Hongmei Li [1], Xiuxiu Lv [1], Jun Yin [4], Huadong Wang [1], Yiyang Wang [1,*]

[1] Department of Pathophysiology, School of Medicine, Jinan University, Guangzhou, Guangdong, China
[2] Department of Pathology, The Third Affiliated Hospital of Southern Medical University, Guangzhou, Guangdong, China
[3] Department of Cardiology, Zhuhai People's Hospital Affiliated with Jinan University, Zhuhai, Guangdong, China
[4] Department of Chemistry, Center for Diagnostics & Therapeutics, Georgia State University, Atlanta, Georgia

ARTICLE INFO

ABSTRACT

Cardiac dysfunction has been recognized as a major contributor to mortality in sepsis, which is closely associated with inflammatory reactions. The carboxy terminus of Hsc70-interacting protein (CHIP), a U-box E3 ubiquitin ligase, defends against cardiac injury caused by other factors, but its role in sepsis-induced cardiac dysfunction has yet to be determined. The present study was designed to investigate the effects of CHIP on cardiac dysfunction caused by sepsis and the molecular mechanisms underlying these processes. We discovered that the CHIP level decreased gradually in the heart at different time points after septic model construction. The decline in CHIP expression of lipopolysaccharide (LPS)-stimulated cardiomyocytes was related to c-Jun activation that inhibited the transcription of CHIP. Functional biology experiments indicated that CHIP bound directly to karyopherin-α 2 (KPNA2) and promoted its degradation through polyubiquitination in cardiomyocytes. CHIP overexpression in cardiomyocytes obviously inhibited LPS-initiated release of TNF-α and IL-6 by promoting KPNA2 degradation, reducing NF-κB translocation into the nucleus. Consistent with the *in vitro* results, data obtained from animal experiments indicated that septic transgenic mice with heart-specific CHIP overexpression showed a weaker proinflammatory response and reduced cardiac dysfunction than septic control mice. Furthermore, we found that the therapeutic effect of compound YL-109 on cardiac dysfunction in septic mice was due to the upregulation of myocardial CHIP expression. These findings demonstrated that sepsis-initiated the activation of c-Jun suppressed CHIP transcription. CHIP directly promoted ubiquitin-mediated degradation of KPNA2, which reduced the production of proinflammatory cytokines by inhibiting the translocation of NF-κB from the cytoplasm into the nucleus in myocardium, thereby attenuating sepsis-induced cardiac dysfunction.

## Introduction

Sepsis is defined as the dysregulation of the host response to infection, which leads to life-threatening organ dysfunction, including multiple organ dysfunction syndrome.[1] Cardiac dysfunction is a common complication associated with increased mortality in septic patients. Several studies have demonstrated that sepsis-induced cardiac dysfunction affects approximately 40% of patients with sepsis and leads to a significant increase in mortality, rate up to 70%.[2,3] Studies with human patients and animal models suggested that pathogen-associated molecular patterns such as lipopolysaccharide (LPS) initiates the nuclear factor κB (NF-κB)-mediated signaling pathway, which induces the release of inflammatory cytokines, including tumor necrosis factor-α (TNF-α) and interleukin-6 (IL-6), resulting in a strong inflammatory response that ultimately leads to myocardial damage.[4-6] Despite recent treatment advances, septic cardiomyopathy remains a common cause of morbidity

*Reprint requests: Yiyang Wang, Department of Pathophysiology, School of Medicine, Jinan University, Huangpu Road No. 601, Guangzhou 510632, Guangdong, China;
*E-mail address:* wangyiyang@jnu.edu.cn (Y. Wang).

[#] These authors contributed equally to this work.

https://doi.org/10.1016/j.trsl.2022.11.006
Received 28 September 2022; Revised 6 November 2022; Accepted 8 November 2022

**At A Glance Commentary**

Liao J, et al.

**Background**

Cardiac dysfunction has been recognized as a major contributor to mortality in sepsis. Carboxy terminus of Hsc70-interacting protein (CHIP) has a protective effect against heart damage caused by other injury factors, but its function in sepsis-induced cardiac injury remains unclear.

**Translational Significance**

Lipopolysaccharide (LPS)-initiated activation of c-Jun, which inhibited CHIP transcription in cardiomyocytes. CHIP directly promoted proteasomal degradation of KPNA2, which suppressed nuclear translocation of NF-$\kappa$B in septic myocardium and then reduced TNF-$\alpha$ and IL-6 release. Cardiac CHIP upregulation exerted a therapeutic effect on sepsis-induced cardiac dysfunction. These findings suggest that restoring cardiac CHIP expression therapies, such as YL-109, may potentially benefit septic patients with cardiac dysfunction.

and mortality worldwide in currently.[7] To improve clinical outcomes and cardiac function, new therapeutic strategies that target the intrinsic mechanisms of sepsis-induced cardiac dysfunction need to be explored.

The carboxyl terminus of Hsp70-interacting protein (CHIP, encoded by the *stub1* gene) is a chaperone-dependent E3 ligase with important functions in the protein quality control system.[8] The CHIP amino acid sequence can be separated into 3 domains, namely, the tetratricopeptide repeat (TPR) domain, charge domain, and U-box domain.[9] CHIP interacts with Hsc/p70 and Hsp90 chaperone proteins through its N-terminal TPR domain and mediates substrate protein ubiquitination through its C-terminal U-box domain.[10] CHIP is highly expressed in heart cells and targets the degradation of proteins critical for multiple cellular functions and signaling pathways.[11,12] Increasing evidence indicates that CHIP has a protective effect against heart damage caused by various injury factors, such as infarction, ischemia, high glucose levels, and doxorubicin exposure.[13-16] However, its function in sepsis-induced cardiac injury remains largely unclear.

The karyopherin superfamily proteins transfer various proteins through the nuclear pore complexes into the nucleus and are critical for both cell physiology and pathophysiology.[17] The karyopherin family comprises karyopherin $\alpha$ and the soluble nuclear transport receptors of the karyopherin $\beta$ subfamily, which possess different structural and functional features.[18] Karyopherin-$\alpha$ 2 (KPNA2), an adaptor protein, is a member of the karyopherin $\alpha$ protein family that plays a crucial role in the transportation of proteins from the cytoplasm into the nucleus.[19] Together with importin-$\beta$, KPNA2 mediates the nuclear translocation of numerous target proteins through nuclear pore complexes via the recognition of nuclear localization signals.[20] The previous study demonstrated that the translocation of NF-$\kappa$B/p65 into the nucleus of cervical tumor and pancreatic acinar cells relies mainly on the canonical KPNA2/importin-$\beta$ pathway.[21,22] Nevertheless, the intricacies underlying the regulation of KPNA2 protein in relation to LPS-induced cardiomyopathies remain unclear. We recently developed a method to identify the ubiquitination substrates of CHIP by designing an orthogonal ubiquitin transfer cascade, in which an engineered ubiquitin is exclusively used by CHIP to label substrate proteins for their subsequent identification by proteomics. In this previous study, Karyopherin beta1 (KPNB1) was identified among potential CHIP substrates.[23] In our current research, we provide convincing evidence supporting the hypothesis that CHIP plausibly promotes the degradation of KPNA2 in the cardiomyocytes through the ubiquitin–proteasome pathway.

In the present study, we found that downregulation of cardiac CHIP expression in septic mice is associated with LPS-induced c-Jun activation. We identified KPNA2 as a substrate of CHIP and found that NF-$\kappa$B entry into the nucleus of cardiomyocytes after LPS stimulation primarily depends on KPNA2. Overexpression of cardiac CHIP inhibits sepsis-induced nuclear import of NF-$\kappa$B by promoting ubiquitin-mediated degradation of KPNA2, which results in reduced production of TNF-$\alpha$ and IL-6, thereby alleviating septic cardiac dysfunction. Furthermore, we found that the therapeutic effect of YL-109 on septic cardiac dysfunction is based on an increase in cardiac CHIP level. These data suggest a novel role for CHIP in mediating KPNA2 ubiquitination and degradation, indicating that CHIP may serve as a potential therapeutic target for cardiac dysfunction in patients with sepsis.

## Materials and Methods

### *Reagents*

A list of the major resources used in this study is provided in the Supplementary material (Supplementary Table S1).

### *Mice*

Wild-type male C57BL/6 mice (8–10 weeks old) weighing 22–25 g were obtained from Guangdong Experimental Animal Center. Rosa26$^{CHIP/+}$ mice were obtained from Shanghai Model Organisms (Shanghai, China). The mice were self-crossed to obtain homozygous Rosa26$^{CHIP/CHIP}$-mice. The mice were genotyped by PCR to determine homozygosity using primers P1 and P2. Rosa26$^{CHIP/CHIP}$ mice were then crossed with Cre-ERT2 mice (Jackson Laboratory) to generate Rosa26$^{CHIP/CHIP}$-Cre mice on a C57BL/6 background. Progeny was screened by PCR for the Cre transgene using primer P3. To generate tamoxifen-inducible cardiac-specific CHIP-overexpressing mice, pharmaceutical grade tamoxifen was dissolved in corn oil at a concentration of 20 mg/mL and given to 2-month-old male Rosa26$^{CHIP/CHIP}$-Cre mice via i.p. injection (100 mg/kg body weight) for 5 consecutive days. There was a 7-day waiting period between the final injection and establishment of the sepsis model. Rosa26$^{CHIP/CHIP}$ mice were treated under the same conditions as the control (Tx-control) mice. The tamoxifen-inducible cardiac-specific CHIP-overexpressing mice were referred to as CHIP OE mice. All the primers for PCR genotyping were listed in the Supplementary material (Supplementary Table S2). All the experimental mice involved in the final analysis were from the same generation.

### *Mouse model procedures*

Cecal ligation and puncture (CLP) and LPS mouse models of sepsis were used in this study. CLP was performed to induce polymicrobial sepsis in mice as previously described.[24] Another mouse model of sepsis was established by intraperitoneal injection with LPS (25 mg/kg, 0.1 mL/10 g body weight). The mice treated intraperitoneally with normal saline (0.1 mL/10 g body weight) were served as controls. Four hours after the CLP procedure or 1 hour after the LPS injection, the mice were injected subcutaneously with normal saline or YL-109. The animals used in this study were handled in strict accordance with the recommendations in the Guide for the Care and Use of Laboratory Animals of the National Institutes of Health. All animal procedures were reviewed and approved by the Animal Ethics Committee of Jinan University (Approval No. IACUC-20220531-01).

### *Echocardiography and measurement of tail artery blood pressure*

Echocardiography was performed under isoflurane anesthesia (2%) using a Vevo770TM high resolution imaging system (VisualSonics, Toronto, Ontario, Canada) 12 hours after LPS injection or 24 hours post-CLP surgery. Transthoracic 2-dimensional M-mode imaging from the parasternal short-axis view at the level of the papillary muscles was performed, and the ascending aortic flow velocity was recorded in continuous Doppler wave mode. The fractional shortening (FS), ejection fraction (EF), stroke volume (SV), cardiac output (CO), and mitral valve

E/A ratio were calculated with Vevo770TM imaging system software. The echocardiography measurements were interpreted by an investigator blinded to the treatments, and the data were averaged on the basis of at least 3 consecutive cardiac cycles. Systolic blood pressure and diastolic blood pressure were recorded in the tails of mice using the noninvasive tail-cuff system (CODA, Kent Scientific Corporation, CT). The mice were pretrained by measuring blood pressure daily for 5 days before the experiments to minimize stress-induced fluctuations.

*Immunohistochemical (IHC) analysis*

All control and septic cardiac tissue samples were fixed in formalin. Paraffin-embedded tissues of the heart were cut into 4-$\mu$m-thick sections using standard techniques. IHC staining was performed as previously described.[25] Briefly, the tissue sections were rinsed with phosphate-buffered saline (PBS) and incubated overnight at 4°C with a monoclonal antibody against CHIP (1:100 dilution) and Ly6G (1:2000 dilution). The slides were washed with PBS and then incubated at room temperature with the appropriate secondary antibody (1:10,000 dilution) for 20 minutes. Diaminobenzidine staining was then performed. The sections were visualized using a microscope (BX45, Olympus Corporation, Tokyo, Japan). The number and intensity of positive cells were identified in 5 randomly selected fields per section viewed at high magnification. Then, the mean value from 5 images per chamber was calculated. The extent of the staining was scored according to the percentage of positive cells as follows: 1, <5%; 2, 5%−25%; 3, 25%−50%; 4, 50%−75%; 5, >75% staining. The intensity score was graded as follows: 0, no staining; 1, weak staining; 2, moderate staining; and 3, strong staining. The final score was calculated using the following formula: total score = percentage score × intensity score. ImageJ software was used to quantify the signal intensity of stained tissues and cells.

*Cell culture*

Neonatal rat cardiomyocytes were isolated from the hearts of 2- to 3-day-old Sprague-Dawley rats (the Laboratory Animal Center of Southern Medical University, Guangzhou, China) according to the methods described in our previous study.[26] The H9c2 (cardiomyoblast) cell line was obtained from the American Type Culture Collection (ATCC). The cells were cultured in Dulbecco's modified Eagle's medium (DMEM) with 10% fetal bovine serum at 37°C with 5% $CO_2$.

*Plasmid construction and transfection*

For reporter assays, the rat species CHIP promoter fragment, from −1 to −1000 in the *stub1* gene, was cloned into a pGL3-Basic Luciferase Reporter vector between restriction sites SmaI and HindIII to obtain a pGL3-CHIP-promoter-Luci luciferase reporter plasmid. pLenti-c-Jun and pLenti-c-Fos plasmids were obtained from IGEBio (Guangdong, China). The pLenti-CHIP plasmid and plasmids constructed for protein expression were kindly provided by Professor Jun Yin from Georgia State University, USA. A Plasmid Midi Kit (QIAGEN) was used for plasmid extraction. Short interfering RNA (siRNA) specific to rat c-Jun, c-Fos, CHIP, and KPNA2 (Sequences refer to Supplementary Table S3) and a scrambled siRNA were purchased from RIBOBIO (Guangdong, China). The plasmids were transfected with Lipofectamine 3000 transfection reagent according to the manufacturer's protocol. Western blot assays were performed to analyze transfection efficiency.

*Western blot analysis*

Tissues and cells were lysed in RIPA buffer containing protease inhibitor to harvest total proteins. Nuclear and cytoplasmic proteins were extracted using a commercially available nuclear and cytoplasmic extraction kit according to the manufacturer's instructions. Western blot experiments were performed as previously described.[27] The proteins were subjected to sodium dodecyl sulfate-polyacrylamide gel electrophoresis and then electrophoretically transferred to polyvinyl difluoride membranes. Following blockage of nonspecific binding sites with 5% nonfat dry milk for 1 hour, the membranes were incubated with the appropriate primary antibodies (1:1000 dilution) overnight at 4°C. After being rinsed with TBST, the membranes were incubated in a 1:20,000 dilution of horseradish peroxidase-conjugated secondary antibody for 1 hour at room temperature. The immunoblotted proteins were visualized with enhanced chemiluminescence reagents. ImageJ software, an open-source image-processing program, was used to quantify the blots.

*Quantitative real-time polymerase chain reaction (QRT-PCR) analysis*

Total RNA was isolated from cells using RNA extraction reagent, and the extracted RNA was reverse transcribed to cDNA using a commercial reverse transcription kit according to the manufacturer's instructions. cDNA was amplified using ChemoHS Q-PCR mix, 0.2 $\mu$M of each primer and nuclease-free water. Amplified cDNA signals were detected and analyzed by CFX Maestro Software v1.1 (Bio-Rad) using $\beta$-Actin as an endogenous control. The QRT-PCR results are expressed as the fold increase compared to the control. Primer sequences for the genes are shown in Supplementary Table S4.

*Immunofluorescence staining*

Primary cardiomyocytes were fixed with 4% formalin solution. The cells were then treated with 0.1% Triton X 100 in PBS to make intracellular protein binding sites more accessible to antibodies. After 3 washes with PBS for 5-minute each time, the cells were blocked in PBS with 1% BSA, followed by incubation with a 1:100 dilution of antibodies at 4°C overnight. The cells were then incubated with Alexa Fluor fluorescent-labeled secondary antibody (1:400 dilution) for 1 hour. Finally, after washing 3 times, the cells were incubated with a 1:200 dilution of 4′,6-diamidino-2-phenylindole (DAPI) for 15 minutes and observed via laser confocal microscopy or fluorescence microscope.

*Dual–luciferase reporter assay*

H9c2 cells seeded on 24-well plates were cotransfected with a pRL-TK, pGL3-CHIP-Luci reporter and pLenti-c-Jun/pLenti-c-Fos plasmids using Lipofectamine 3000 transfection reagent, following the manufacturer's protocol. Dual luciferase activity in total cell lysates was measured 48 hours after transfection with a Dual-Luciferase Reporter Assay System according to the manufacturer's instructions. The relative activity was normalized by the ratio of firefly luciferase activity to Renilla luciferase activity (the internal control).

*Cell counting kit-8 (CCK-8) assay*

After treatment with drugs, cell proliferation was quantified by CCK-8 assay according to the standard protocol. Briefly, neonatal rat cardiomyocytes were seeded into 96-well plates at a density of $1 \times 10^4$ cells/mL in 100 $\mu$L of suspension and then treated with drugs for 48 hours. The plate was incubated for an appropriate length of time in an incubator. Ten microliters of CCK-8 solution was added to each well and incubated for 2 hours at 37°C. The optical density (OD) at 450 nm was detected utilizing an Epoch 2 Microplate Spectrophotometer (BioTek Instruments, Winooski, VT).

*Enzyme-linked immunosorbent assay (ELISA)*

The TNF-$\alpha$ and IL-6 levels were detected by using ELISA kits (R&D Systems, Inc., Minneapolis, MN) according to the manufacturer's instructions.

*Protein expression and purification*

pET expression plasmids for use in *in vitro* ubiquitination assays were constructed following the procedures described in a previous study.[23] Chemically competent *Escherichia coli* BL21 cells were transformed with pET expression plasmids and plated on LB agar plates with the appropriate antibiotics. Protein expression and purification assays were performed following the instructions from the respective manufacturer of the pET expression system and Ni-NTA agarose resin.

*In vitro KPNA2 ubiquitination assays*

All ubiquitination assays were performed in 30 $\mu$L of TBS supplemented with 10 mM $MgCl_2$ and 1.5 mM ATP. In each UB transfer reaction, 5 $\mu$M KPNA2 was incubated with 1 $\mu$M Uba1, 5 $\mu$M UbcH7, 10 $\mu$M CHIP, and 20 $\mu$M ubiquitin (Ub) for 4 hours at 30°C. The reactions were quenched by boiling in Laemmli buffer with BME and analyzed by Western blot probed with anti-KPNA2 antibody.

*Coimmunoprecipitation assays*

Cardiomyocytes were washed with ice-cold PBS and then lysed in RIPA lysis buffer. The supernatant was obtained by centrifugation and then incubated with 2 $\mu$g of a primary antibody against KPNA2 for 1 hour at 4°C. After incubation, the supernatant was added to 50 $\mu$L of Protein A/G PLUS-Agarose beads and incubated at 4°C overnight. The beads were then washed 3 times with lysis buffer. After the final wash, the beads were resuspended in 40 $\mu$L of 1 × Laemmli buffer with BME. The samples were boiled for 5 minutes and analyzed by Western blot with antibodies specific to the target proteins.

*Cycloheximide (CHX) chase assay*

CHX chase assays were used to examine the effects of CHIP on KPNA2 stability. H9c2 cells ($8 \times 10^5$ cells) were transfected with empty pLenti, pLenti-CHIP and CHIP siRNA plasmids separately to increase or decrease the expression of CHIP. After 48 hours, the cells were treated with 100 $\mu$g/mL CHX to block further protein synthesis, as previously described.[28] Cells were harvested at consecutive time points (0, 2, 4, and 8 hours) after CHX incubation, and whole-cell lysates were analyzed by immunoblotting for CHIP and KPNA2 detection.

*Statistical analysis*

All quantitative data are presented as the mean ± standard error of the mean (SEM). Comparisons among groups with normally distributed data were analyzed using ordinary one-way ANOVA with Dunnett's, Holm-Sidak, or Tukey's multiple comparison test. Data showing nonnormal distribution were examined by Wilcoxon matched-pairs signed-rank test, Mann-Whitney test, or Kruskal-Wallis with Dunn's multiple comparisons test. Differences with $P < 0.05$ were considered statistically significant. SPSS software was used to analyze the data. All experiments were performed in a randomized manner, and data analysis was performed in a blinded manner with the name and allocation schemes concealed.

## Results

*The protein and mRNA levels of CHIP are reduced in the hearts of septic mice and LPS-stimulated primary neonatal cardiomyocytes*

To determine the functional role of cardiac CHIP in response to sepsis, we first examined CHIP expression in the cardiac tissue of septic mouse models established separately via CLP and intraperitoneal LPS injection. QRT-PCR and Western blot were performed to determine CHIP mRNA and protein expression in the heart at different time points after septic model construction. The results showed that the protein and mRNA levels of CHIP in myocardial tissue were gradually decreased in the CLP mouse model after 4 hours (Fig 1, *A* and *B*). The expression of CHIP protein and mRNA in the myocardium was significantly lower 1 hour after the intraperitoneal injection of LPS and dropped rapidly from 4 hours after LPS stimulation (Fig 1, *C* and *D*). CHIP staining in the myocardium of the septic mice was also measured by IHC analysis after CLP surgery or LPS stimulation for 4 hours. As depicted in Fig 1, *E* and *F*, CHIP immunostaining was significantly weaker in cardiac tissues of the septic mice than that in the control mice. We also counted CHIP-positive cells and calculated the pathological scores associated with CHIP expression. Our analysis confirmed that the number of CHIP-positive cells and corresponding pathological scores were obviously lower in the myocardium of both the CLP- and LPS-challenged mice than compared with that of the control mice. To further confirm the effect of LPS on CHIP expression *in vitro*, neonatal rat cardiomyocytes were isolated and treated with LPS at different concentrations. The protein expression of CHIP was reduced in an LPS dose-dependent manner and markedly decreased after LPS treatment for 4 hours at concentrations greater than 0.1 $\mu$g/mL (Fig 1, *G*). The mRNA level of CHIP was decreased after LPS stimulation for 2 hours at different concentrations and was similar to the change in CHIP protein expression (Fig 1, *H*). The immunofluorescence results also showed that the expression of CHIP was reduced 4 hours after 1 $\mu$g/mL LPS stimulation (Fig 1, *I*). Therefore, we chose LPS at a concentration of 1 $\mu$g/mL for subsequent experiments. These results indicated that the protein and mRNA expression levels of CHIP were decreased in both the hearts of the septic mice and LPS-stimulated cardiomyocytes.

*The effect of c-Jun on negatively regulating CHIP transcription mediates LPS-induced CHIP suppression*

Studies have reported that LPS activates several signaling pathways that promote the nuclear import of transcription factors, such as c-Fos/c-Jun and NF-κB, regulating downstream gene expression.[29,30] To determine whether the activation of c-Fos/c-Jun and NF-κB inhibits the expression of CHIP, neonatal cardiomyocytes were pretreated with the JNK/c-Fos/c-Jun inhibitor SP600125 (50 $\mu$M) or the NF-κB inhibitor PDTC (50 $\mu$M) for 15 minutes prior to LPS stimulation. As shown by the results in Fig 2, *A*–*C*, SP600125 decreased both c-Jun and c-Fos activation and led to almost full recovery of the CHIP protein and mRNA levels in cardiomyocytes after LPS stimulation. Although PDCT reduced the level of nuclear NF-κB, it exerted no effect on the expression of CHIP in the LPS-treated cardiomyocytes. To detect whether both c-Jun and c-Fos are negative regulators of CHIP transcription, we performed a dual-luciferase reporter assay. The results showed that overexpression of c-Jun, but not c-Fos, significantly decreased the luciferase activity of the CHIP promoter compared with that in the control group (Fig 2, *D*). Subsequently, the expression of CHIP was detected in c-Jun or c-Fos knockout cells. The results of Western blot and QRT-PCR suggested that knockout of c-Jun upregulated both the protein and mRNA levels of CHIP in the LPS-treated cardiomyocytes. However, CHIP expression was not affected by the change in c-Fos content (Fig 2, *E*–*G*). Immunofluorescence assays confirmed that the expression of CHIP was significantly increased in c-Jun knockout cardiomyocytes compared to that in wild-type cardiomyocytes after LPS stimulation for 4 hours, as determined by analyzing fluorescence intensity (Fig 2, *H*). Therefore, these data proved that the activation of c-Jun directly targeted and suppressed CHIP expression at the transcriptional level in cardiomyocytes after LPS stimulation.

*CHIP negatively regulates the stability of KPNA2 in cardiomyocytes through the ubiquitin-proteasome pathway*

We have demonstrated the changing trend of CHIP expression in cardiomyocytes after LPS stimulation. The expression and ubiquitination of KPNA2 in LPS-stimulated cardiomyocytes were further investigated by Western blot and immunoprecipitation. The Western blot results showed

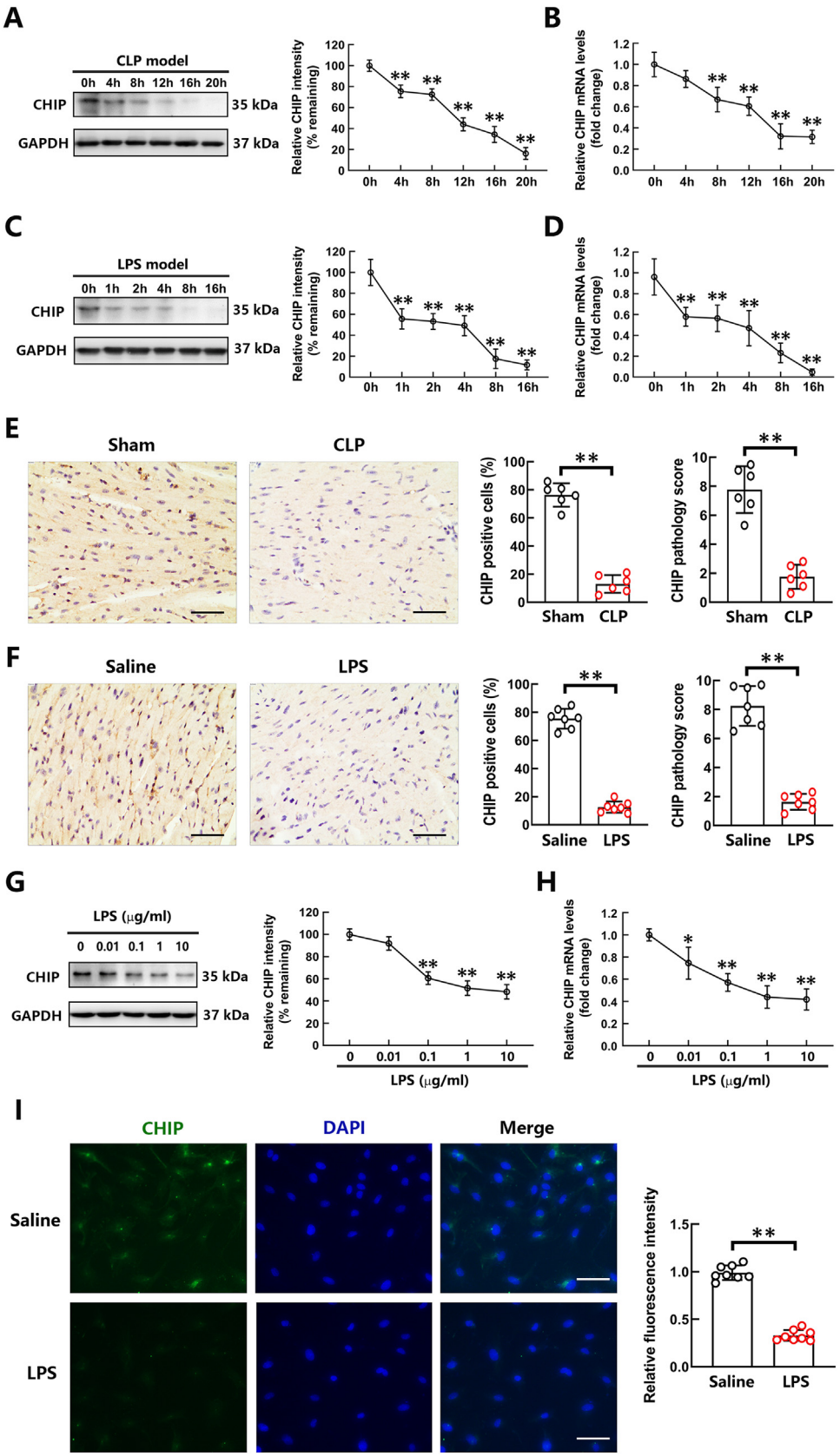


**Fig 1.** The expression of CHIP in the cardiac tissue of septic mice and LPS-stimulated primary neonatal cardiomyocytes. (A–D) The protein (A&C) and mRNA (B&D) levels of CHIP in the cardiac tissues at different time points after CLP (A&B) and LPS (C&D) septic model construction. Quantifications of CHIP protein levels are shown on the right-hand side of the images. (E and F) Representative IHC images showing CHIP staining in the heart tissues of CLP-treated (E) and LPS-treated (F) mice. Scale bar = 200 $\mu$m. The percentages of CHIP-positive cells and the pathology scores for CHIP-positive staining, on the right-hand side of the images, were calculated based on 5 randomly selected fields of stained cardiac tissues from control and septic mice. (G) The protein expression of CHIP in neonatal rat cardiomyocytes treated with

that the level of KPNA2 was increased, which was a trend opposite CHIP expression in neonatal cardiomyocytes after LPS stimulation for 2 hours and 4 hours (Fig 3, *A*). The immunoprecipitation results showed that LPS decreased the ubiquitination of KPNA2, resulting in significantly increased KPNA2 expression in cardiomyocytes. CHIP directly interacted with KPNA2 in cardiomyocytes, and the interactions were reduced upon LPS treatment (Fig 3, *B*). To confirm that CHIP plays a direct role in regulating KPNA2 levels in cardiomyocytes, we transfected H9c2 cells with siRNA against CHIP or pLenti-CHIP to knock out or overexpress CHIP. The cells were treated with the proteasome inhibitor MG132 (10 $\mu$M) before harvesting to inhibit protein degradation. The specific antibody was used to immunoprecipitate KPNA2, and an anti-ubiquitin antibody was used to determine its ubiquitination level. As shown in Fig 3, *C*, a decreased level of ubiquitinated KPNA2 in H9c2 cardiomyocytes expressing siRNA against CHIP was observed. Overexpression of CHIP increased the level of ubiquitinated KPNA2 in H9c2 cells. We then purified the ubiquitin (Ub), Uba1 (E1), Ubch7 (E2), CHIP, and KPNA2 proteins expressed in *E. coli* and used them to perform ubiquitination reactions *in vitro*. The polyubiquitination of KPNA2 was observed when Ub was transferred through the Uba1-UbcH7-CHIP cascade (Fig 3, *D*). Furthermore, after CHIP expression was sequentially increased in H9c2 cells, we measured KPNA2 levels by Western blot. The overexpression of CHIP significantly decreased levels of KPNA2 in H9c2 cells (Fig 3, *E*). We also inhibited protein synthesis by adding 100 $\mu$g/mL cycloheximide (CHX) and compared the rate of KPNA2 degradation in H9c2 cardiomyocytes with CHIP overexpression or knockout. The results showed that overexpression of CHIP accelerated the degradation of KPNA2 in H9c2 cardiomyocytes. Decreased CHIP expression induced by siRNA extended the stability of KPNA2 in H9c2 cells (Fig 3, *F*). These results confirmed the negative correlation between CHIP and KPNA2 levels in cardiomyocytes. CHIP directly downregulated the stability of KPNA2 in myocardial cells via ubiquitination and proteasomal degradation.

### *Upregulation of CHIP inhibits LPS-induced release of TNF-α and IL-6 by downregulating KPNA2-mediated translocation of NF-κB into the nucleus of cardiomyocytes*

KPNA2, an important karyopherin, has been implicated in the regulation of NF-κB nuclear import in HeLa and pancreatic acinar cells.[21,22] This study next sought to determine whether LPS-induced nuclear transport of NF-κB is regulated by KPNA2 in cardiomyocytes. We knocked down KPNA2 in H9c2 cells via siRNA transfection and then measured the levels of NF-κB in the cytoplasm and nucleus of cells stimulated by LPS for 4 hours. As shown in Fig 4, *A*, a decreased content of NF-κB in the cytoplasm and correspondingly an amplifying level in the nucleus of LPS-treated cells were observed. Knockdown of KPNA2 blocked NF-κB transport from the cytoplasm to the nucleus. The immunofluorescence assay results showed that significant NF-κB staining was localized to the nucleus after LPS stimulation of cardiomyocytes. However, the immunoreactivity of nuclear NF-κB was significantly attenuated in cells transfected with KPNA2 siRNA, which correlated with diminished levels of KPNA2 (Fig 4, *B*). Moreover, KPNA2 knockdown significantly inhibited the release of TNF-α and IL-6 from cardiomyocytes stimulated with LPS for 24 hours (Fig 4, *C*). To further examine the direct correlation between KPNA2 and NF-κB, H9c2 cells lysates were immunoprecipitated with anti-KPNA2 antibody, followed by Western blot for detecting the NF-κB level after LPS stimulation for 2 hours and 4 hours. We found that KPNA2 directly interacted with NF-κB in cardiomyocytes, and the correlation between KPNA2 and NF-κB was enhanced upon LPS stimulation (Fig 4, *D*). LPS initiates the nuclear translocation of NF-κB, resulting in the activation of its downstream genes and release of cytokines such as TNF-α and IL-6.[31] We therefore postulated that KPNA2 degradation induced by CHIP limits the production of TNF-α and IL-6 by restricting the rate of NF-κB nuclear translocation. To test this hypothesis, we transfected 1$\mu$g/well pLenti-CHIP and empty vector plasmids separately into H9c2 cells in the 6-well plate and treated the cells with LPS for 4 hours. The Western blot results confirmed that CHIP overexpression significantly reversed the elevation in KPNA2 level and increased nuclear translocation of NF-κB induced by LPS (Fig 4, *E*). Interestingly, overexpression of CHIP did not affect either LPS-induced elevation in the total cellular NF-κB or phosphorylation of IκBα (Fig 4, *E*). Furthermore, knockdown of CHIP increased the nuclear transport of NF-κB without affecting cellular total NF-κB level in LPS-stimulated H9c2 cells (Supplementary Fig S1, *A* and *B*). We then measured the levels of TNF-α and IL-6 in the supernatant of H9c2 cells after LPS stimulation for 24 hours. As shown in Fig 4, *F* and *G*, elevated CHIP expression significantly reduced LPS-induced release of TNF-α and IL-6 from H9c2 cells. These observations indicated that CHIP upregulation inhibited the increase in KPNA2 and nuclear translocation of NF-κB upon LPS stimulation, resulting in the suppression of TNF-α and IL-6 production in cardiomyocytes.

### *Heart-specific CHIP overexpression attenuates cardiac dysfunction in septic mice by reducing the levels of nuclear NF-κB and downregulating TNF-α and IL-6 release*

To evaluate whether increased CHIP expression protects against septic cardiac dysfunction *in vivo*, mice with cardiomyocyte-specific CHIP overexpression (CHIP OE) were used to establish CLP- and LPS-induced sepsis models. The genotype of the transgenic mice was confirmed by PCR with DNA obtained via tail biopsy (Supplementary Fig S2, *A*). The CHIP expression in multiple organs of the mice was measured by Western blot, and the results showed that the levels of cardiac CHIP protein were much higher in the CHIP OE mice than that in the Tx-control mice. No significant difference in CHIP expression in other tissues between CHIP OE and Tx-control mice was observed (Supplementary Fig S2, *B*). The cardiac function of CHIP OE and Tx-control mice was evaluated by echocardiography 12 hours after LPS injection and 24 hours post-CLP surgery. Fig 5, *A* and *C* showed representative M-mode echocardiograms after control or septic model establishment with Tx-control and CHIP OE mice. Septic mice were found to display a marked decrease in left ventricular fractional shortening and ejection fraction (FS and EF), whereas these alterations were markedly restored in CHIP OE mice. Moreover, LPS or CLP treatment caused a pronounced reduction in cardiac diastolic function of Tx-control mice, as reflected by the E/A ratio, and this effect was significantly attenuated in CHIP OE mice (Fig 5, *B* and *D*). Representative Doppler-derived mitral inflow images used to calculate E/A ratios were shown in the Supplementary Materials (Supplementary Fig S3, *A* and *B*). In addition, the SV, CO, systolic blood pressure and diastolic blood pressure were significantly higher in the CHIP OE septic mice than that in the Tx-control septic mice (Supplementary Fig S4, *A* and *B*). The survival curves showed that overexpression of CHIP in the heart reduced the mortality in septic mice (Supplementary Fig S4, *C*). To determine the role of cardiac CHIP overexpression in the production of proinflammatory cytokines, the contents of cardiac TNF-α and IL-6 after LPS injection for 4 hours or CLP for 20 hours were measured by ELISA. The ELISA results showed that the sepsis-initiated increased levels of TNF-α and IL-6 were significantly alleviated in the hearts with CHIP overexpression (Fig 5, *E* and *F*). Furthermore, the alterations in cardiac KPNA2 expression and nuclear NF-κB level in septic mice were confirmed upon overexpression of cardiac CHIP. As shown in Fig 5, *G* and

LPS at different concentrations for 4 hours. Quantification of the relative CHIP level is shown on the right-hand side of the images. (H) The CHIP mRNA level in cardiomyocytes treated with LPS at different concentrations for 2 hours was measured by QRT-PCR analysis. (I) Representative immunofluorescence photomicrographs showing CHIP expression (green) in cardiomyocytes stimulated with saline (upper) and LPS (1 $\mu$g/mL, bottom) for 4 hours. Complete nuclei were stained with DAPI (blue). Scale bar = 100 $\mu$m. The relative CHIP fluorescence intensity is shown on the right-hand side of the images. Data are presented as mean ± SEM. $n = 5–8$; $^{*}P < 0.05$, $^{**}P < 0.01$ versus control group. (For interpretation of the references to color in this figure legend, the reader is referred to the Web version of this article.)

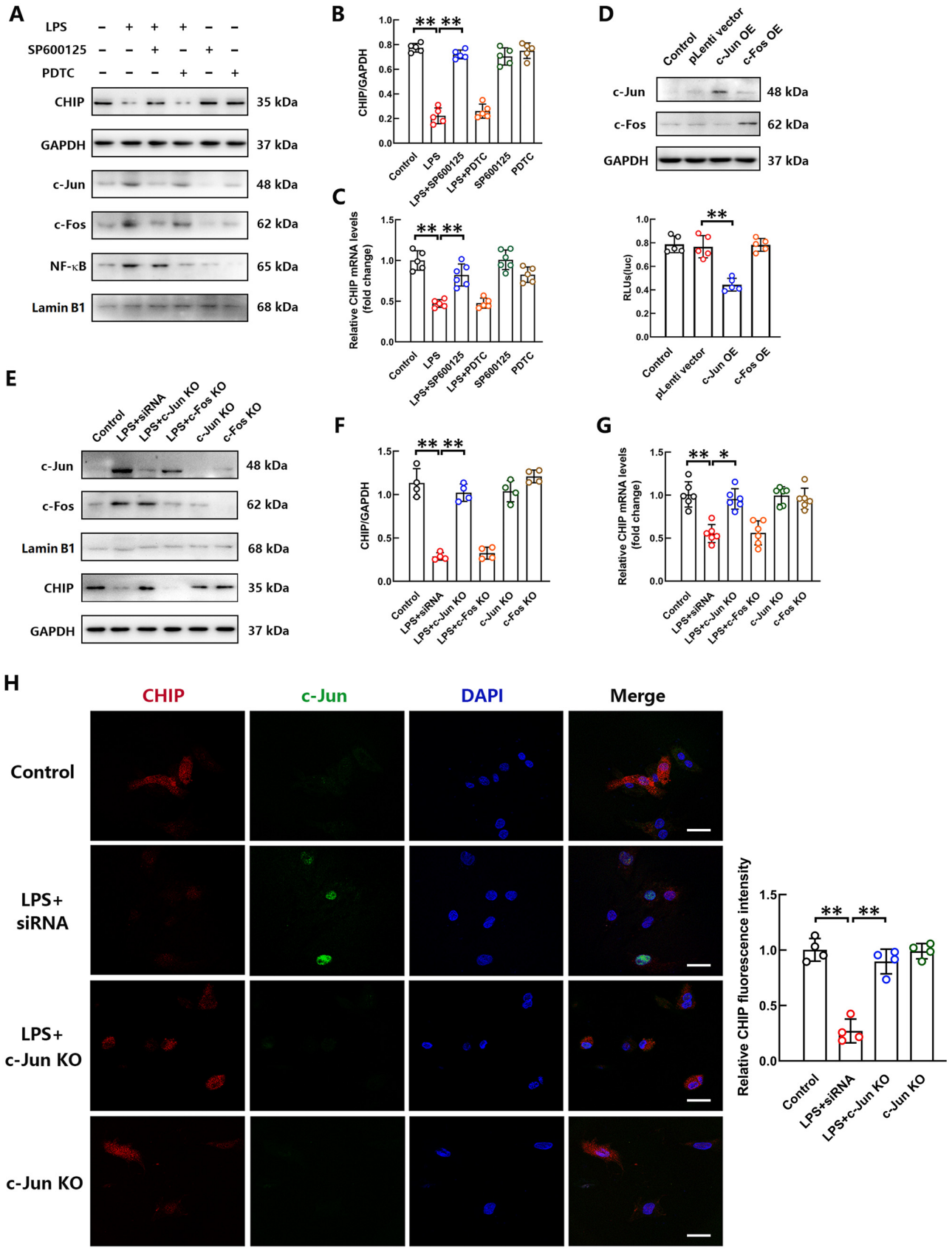


**Fig 2.** c-Jun decreased the transcriptional activity of CHIP in cardiomyocytes treated with LPS. (A) CHIP, c-Jun, c-Fos, and NF-κB protein expression in cardiomyocytes stimulated with LPS, SP600125, or PDTC was measured by Western blot. (B) Quantification of the CHIP intensity in Western blot. (C) The mRNA level of CHIP in cardiomyocytes treated with LPS, SP600125, or PDTC. (D) The relative dual-luciferase activity of CHIP promoter in cardiomyocytes with c-Jun or c-Fos overexpression (bottom). c-Jun and c-Fos expression in cardiomyocytes transfected with the associated overexpression plasmids (upper). (E) CHIP, c-Jun, and c-Fos protein expression in cardiomyocytes after transfection with c-Jun or c-Fos siRNA. (F) Quantification of the CHIP intensity in Western blot. (G) CHIP mRNA levels in c-Jun- or c-Fos-

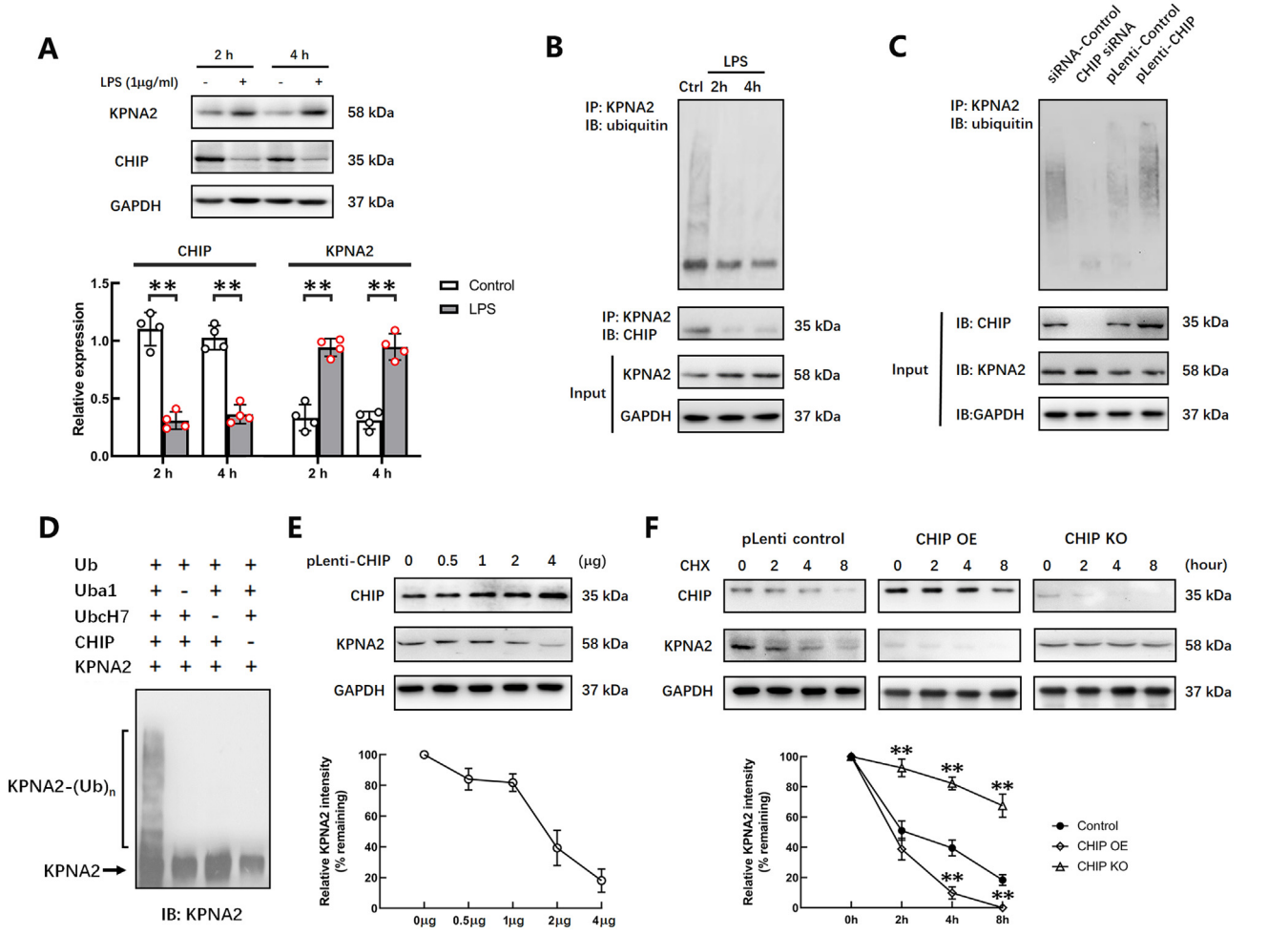


**Fig 3.** CHIP downregulated the expression of KPNA2 in cardiomyocytes through ubiquitin-proteasome pathway. (A) The expression of CHIP and KPNA2 in cardiomyocytes with or without LPS stimulation for 2 hours and 4 hours. Quantification of the relative CHIP and KPNA2 levels are shown at the bottom of the images. (B) Coimmunoprecipitation and Western blot analysis for ubiquitination of KPNA2 and association between KPNA and CHIP in cardiomyocytes after LPS treatment for 2 hours and 4 hours. (C) Ubiquitination of KPNA2 in H9c2 cells with CHIP knocked out or overexpressed. (D) Ubiquitination reactions were performed with ubiquitin (Ub), Uba1, UBcH7, CHIP, and KPNA2 proteins *in vitro*. KPNA2 ubiquitination levels were detected by Western blot analysis. (E) The levels of KPNA2 in H9c2 cells transfected with increasing amounts of pLenti-CHIP. Quantification of the relative KPNA2 level is shown at the bottom of the images. (F) H9c2 cells were transfected with pLenti control, pLenti-CHIP, or CHIP siRNA and then treated with cycloheximide (CHX, 100 $\mu$g/mL). Cell extracts were collected 0, 2, 4, and 8 hours after incubation with CHX, and then, the proteins were measured by Western blot. Quantitative analysis of the relative KPNA2 level is shown at the bottom of the images. Data are presented as mean ± SEM. $n = 4$-5; $^*P < 0.05$, $^{**}P < 0.01$. (For interpretation of the references to color in this figure legend, the reader is referred to the Web version of this article.)

*H*, the cardiac expression of KPNA2 and NF-κB activation were significantly increased in the septic mice treated by LPS or CLP. Conversely, these changes were markedly attenuated in the heart with CHIP overexpression of septic mice. Together, these results indicated that overexpression of CHIP ameliorated cardiac functional deterioration and survival of mice in response to sepsis, which was associated with inhibition of TNF-α and IL-6 release by suppressing the elevation of KPNA2 and NF-κB nuclear import.

### *The inhibitory effect of YL-109 on LPS-induced TNF-α and IL-6 release depends on the upregulation of CHIP expression in cardiomyocytes*

Although the ameliorating effect of CHIP on septic cardiac dysfunction was demonstrated, we still needed to explore agents that upregulate CHIP expression to suggest new strategies for clinical treatment. A previous study demonstrated that 2-(4-hydroxy-3-methoxyphenyl)-benzothiazole (YL-109, Fig 6, *A*) increased CHIP expression by recruiting AhR to the promoter region of the *CHIP* gene in breast cancer cells.[32] To further explore whether YL-109 upregulates the expression of CHIP in LPS-treated cardiomyocytes, different concentrations of YL-109 were administered to H9c2 cells 15 minutes prior to LPS stimulation. The levels of CHIP were obviously elevated in the LPS-stimulated cells after YL-109 treatment at concentrations of 1 $\mu$M and 10 $\mu$M, and the effects of these 2 concentrations were similar (Fig 6, *B*). Furthermore, YL-109 administered at doses of 1 $\mu$M and 10 $\mu$M, but not at 0.1 $\mu$M, markedly reduced the levels of TNF-α and IL-6 secreted from H9c2 cells after LPS stimulation for 24 hours (Fig 6, *C*). The results of CCK-8 assay indicated that, compared with the viability of H9c2 cells in the control group, no significant difference in the viability of cells was observed after treatment with 1 $\mu$g/mL LPS and different doses of YL-109 for 24 hours

knockout cardiomyocytes after LPS or saline stimulation. (H) Immunofluorescence images showing CHIP expression in c-Jun-knockout cardiomyocytes with or without LPS challenge. Cardiomyocytes were stained with antibodies against CHIP (red) and c-Jun (green). Complete nuclei were stained with DAPI (blue). Scale bar = 50 $\mu$m. Quantification of relative CHIP fluorescence intensity is shown on the right-hand side of the images. Data are presented as mean ± SEM. $n = 4$-6; $^*P < 0.05$, $^{**}P < 0.01$. (For interpretation of the references to color in this figure legend, the reader is referred to the Web version of this article.)

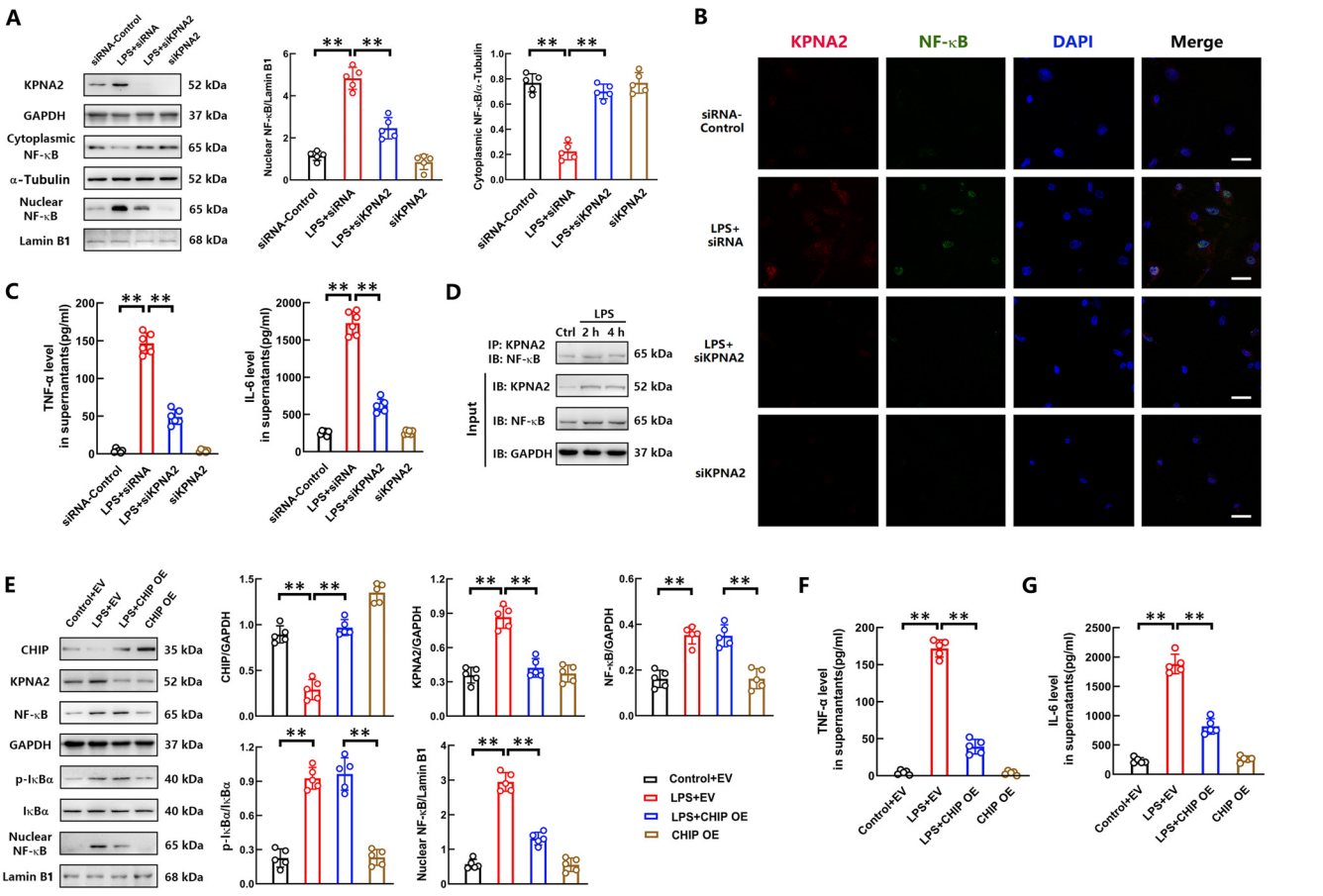


**Fig 4.** CHIP inhibited LPS-induced TNF-$\alpha$ and IL-6 production in cardiomyocytes by reducing KPNA2-mediated nuclear translocation of NF-$\kappa$B. (A) NF-$\kappa$B levels in the cytoplasm and nucleus of KPNA2-knockout H9c2 cells treated with LPS. Quantifications of NF-$\kappa$B levels are shown on the right-hand side of the images. (B) Representative immunofluorescence image showing NF-$\kappa$B in KPNA2-knockout H9c2 cells with or without LPS challenge. H9c2 cells were stained with antibodies against KPNA2 (red) and NF-$\kappa$B (green). Complete nuclei were stained with DAPI (blue). Scale bar = 50 $\mu$m. (C) TNF-$\alpha$ and IL-6 levels in the supernatants of KPNA2-knockout H9c2 cells stimulated with LPS for 24 hours. (D) The correlation between KPNA2 and NF-$\kappa$B was determined via coimmunoprecipitation and Western blot analysis. (E) The levels of KPNA2, p-I$\kappa$B$\alpha$, total NF-$\kappa$B, and nuclear NF-$\kappa$B in H9c2 cells overexpressing CHIP after LPS or saline stimulation. Quantifications of the relative protein levels are shown on the right-hand side of the images. (F and G) TNF-$\alpha$ (F) and IL-6 (G) levels in the supernatants of CHIP-overexpressing H9c2 cells stimulated with LPS or saline for 24 hours. Data are presented as mean ± SEM. $n$ = 5-6; $^*P < 0.05$, $^{**}P < 0.01$. (For interpretation of the references to color in this figure legend, the reader is referred to the Web version of this article.)

(Supplementary Fig S5). These outcomes corroborated that the expression of CHIP showed a trend opposite to the release of TNF-$\alpha$ and IL-6 in the cardiomyocytes treated with LPS. After LPS stimulation for 2 hours, 1 $\mu$M YL-109 markedly increased CHIP mRNA expression in H9c2 cells (Fig 6, *D*). CHIP upregulation has been shown to reduce LPS-induced TNF-$\alpha$ and IL-6 release by inhibiting the KPNA2/NF-$\kappa$B axis activation in cardiomyocytes (Fig 4). Therefore, we explored the potential effect of YL-109 on the levels of KPNA2 and nuclear NF-$\kappa$B in H9c2 cells treated with LPS for 4 hours. As shown in Fig 6, *E*, YL-109 significantly eliminated the LPS-induced elevation of KPNA2 in H9c2 cells. The nuclear import of NF-$\kappa$B activated by LPS in cardiomyocytes was reduced upon YL-109 treatment in parallel with KPNA2. To investigate whether the effects of YL-109 in LPS-stimulated cardiomyocytes depend on CHIP expression, siRNA against CHIP was transfected into H9c2 cells to knockdown CHIP. The results showed that the suppressive effect of YL-109 on KPNA2 expression was reversed by CHIP knockdown in H9c2 cells treated with LPS (Fig 6, *F*). The inhibitory role of YL-109 in LPS-induced NF-$\kappa$B nuclear localization was also abolished by downregulation of CHIP (Fig 6, *G*). Moreover, the inhibitory effect of YL-109 on LPS-induced TNF-$\alpha$ and IL-6 release was lost in CHIP-knockout H9c2 cells (Fig 6, *H* and *I*). These data indicated that the effect of YL-109 on inhibiting LPS-initiated production of TNF-$\alpha$ and IL-6 in the cardiomyocytes was depended on increased CHIP expression. It suggests that YL-109 may alleviate septic cardiac dysfunction through its anti-inflammatory effects by upregulating cardiac CHIP.

*YL-109-mediated elevation of cardiac CHIP expression alleviates cardiac dysfunction in septic mice by inhibiting KPNA2 expression and NF-$\kappa$B activation*

Using mouse model of sepsis induced by LPS injection, we subcutaneously injected different doses of YL-109 (1/10/50 mg/kg weight) 1 hour after LPS stimulation and then investigated the effect of YL-109 on the regulation of myocardial CHIP expression *in vivo*. YL-109 injected at dose of 1 mg/kg partially restored the level of myocardial CHIP, and 10 mg/kg and 50 mg/kg doses of YL-109 increased cardiac CHIP expression more significantly in the mice 2 hours after LPS challenge (Fig 7, *A*). Moreover, the 10 mg/kg and 50 mg/kg doses of YL-109 led to a more significant reduction in TNF-$\alpha$ and IL-6 levels in the myocardium of the mice 4 hours after LPS injection. The difference between the 10 mg/kg and 50 mg/kg doses was not statistically significant (Fig 7, *B* and *C*). In addition, YL-109 injected at a dose of 10 mg/kg upregulated the expression of CHIP at the transcriptional level in the hearts of the mice 2 hours after LPS treatment (Fig 7, *D*). Therefore, we selected 10 mg/kg dose of YL-109 for subsequent animal experiments. We found that YL-109 inhibited the elevation of KPNA2 and the activation of NF-

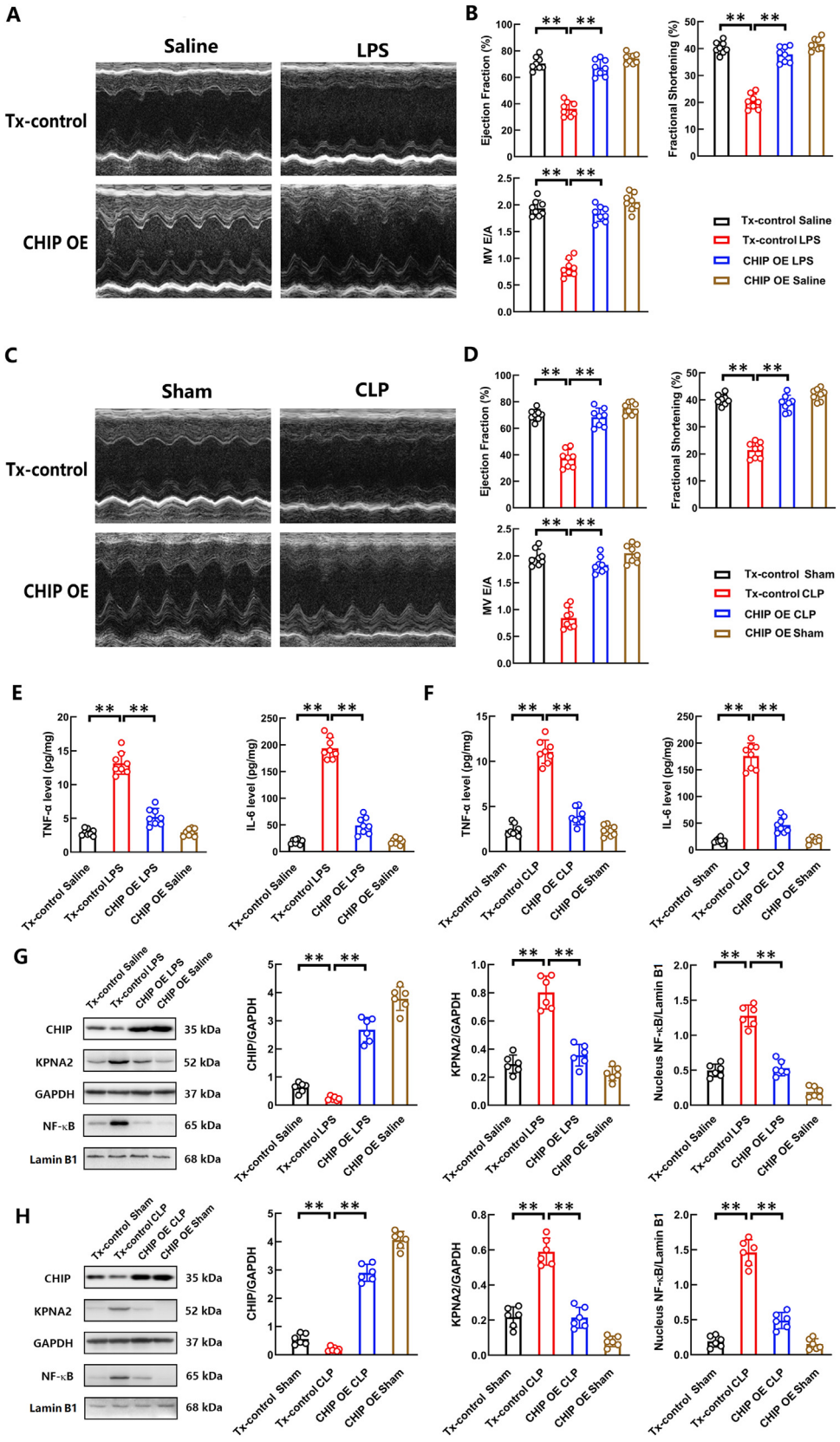


**Fig 5.** Heart-specific overexpression of CHIP prevented sepsis-induced cardiac dysfunction by inhibiting TNF-$\alpha$ and IL-6 production in cardiac tissues of mice. (A) Representative M-mode echocardiograms of Tx-control and CHIP OE mice treated with saline or LPS for 12 hours. (B) Quantitative group data for echocardiographic measurements: ejection fraction, fractional shortening and E/A ratio. (C) Representative M-mode echocardiograms of Tx-control and CHIP OE mice treated with sham or CLP for 24 hours. (D) Quantitative group data for echocardiographic measurements: ejection fraction, fractional shortening and mitral valve E/A ratio (MV E/A). (E) The levels of cardiac TNF-$\alpha$ and IL-6 in saline- or LPS-stimulated Tx-control and CHIP OE mice for 4 hours. (F) The contents of cardiac TNF-$\alpha$ and IL-6 in Tx-control and CHIP OE mice treated with CLP for 20 hours. (G and H) The levels of cardiac CHIP, KPNA2, and nuclear NF-$\kappa$B in Tx-control and CHIP OE mice after LPS (G) and CLP (H) challenge. Quantifications of the relative protein levels are shown on the right-hand side of the images. Data are presented as mean ± SEM. $n = 6–8$; $^*P < 0.05$, $^{**}P < 0.01$. (For interpretation of the references to color in this figure legend, the reader is referred to the Web version of this article.)

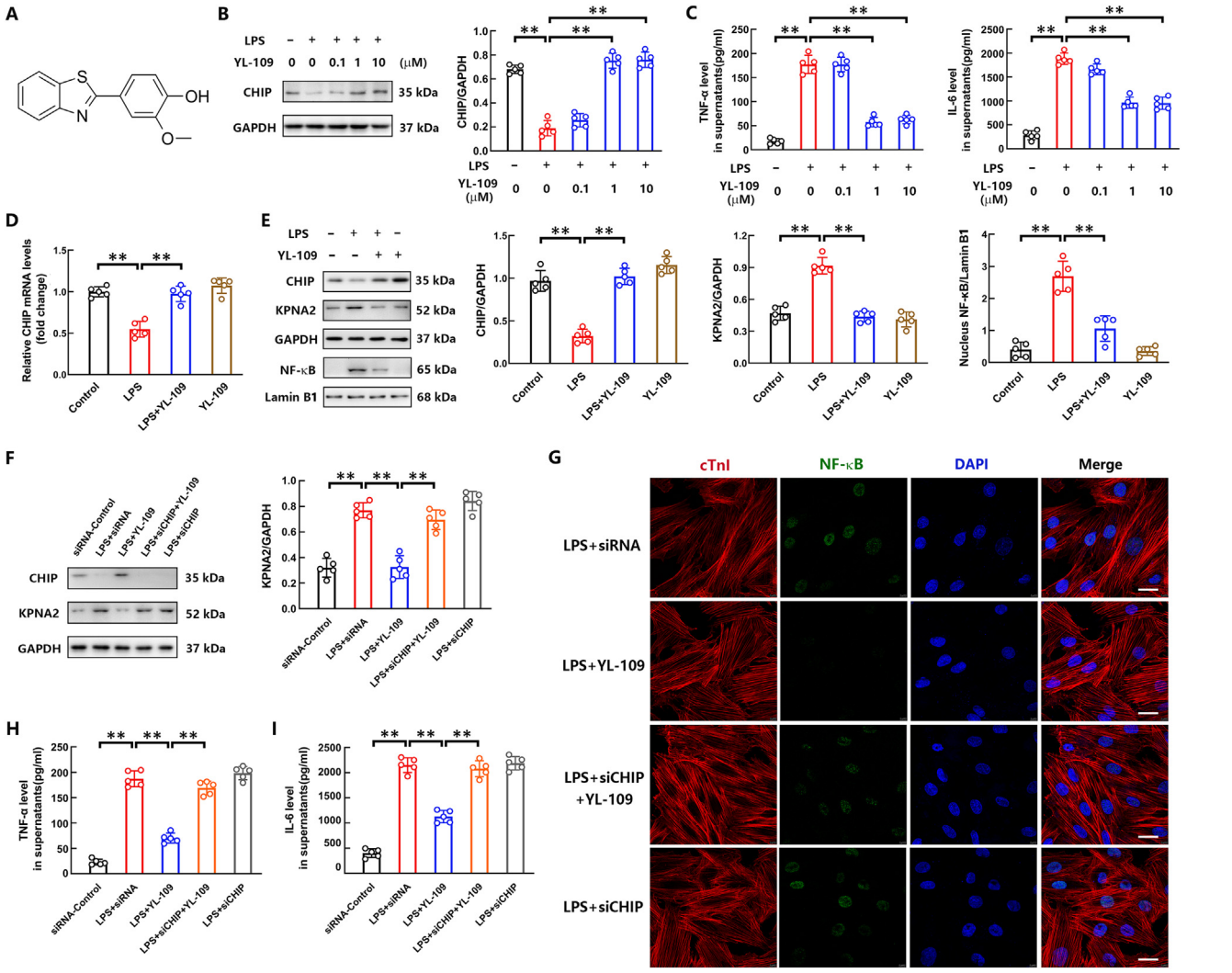


**Fig 6.** YL-109 alleviated the LPS-induced increase in TNF-$\alpha$ and IL-6, which depended on upregulated CHIP expression in cardiomyocytes. (A) Structure of 2-(4-hydroxy-3-methoxyphenyl)-benzothiazole, YL-109. (B) The protein expression of CHIP in H9c2 cells treated with LPS and different concentrations of YL-109 for 4 hours. Quantification of the relative CHIP levels are shown on the right-hand side of the images. (C) TNF-$\alpha$ and IL-6 levels in the supernatants of H9c2 cells stimulated with LPS and YL-109 at different concentrations for 24 hours. (D) CHIP mRNA expression in H9c2 cells treated with LPS and/or YL-109 (1 $\mu$M) for 2 hours. (E) The levels of CHIP, KPNA2, and nuclear NF-$\kappa$B in H9c2 cells after LPS and/or YL-109 stimulation for 4 hours. Quantifications of the relative protein levels are shown on the right-hand side of the images. (F) The expression of KPNA2 in CHIP-knockdown H9c2 cells challenged with LPS and/or YL-109 for 4 hours. (G) Representative confocal images showing nuclear NF-$\kappa$B expression in CHIP-knockdown H9c2 cells stimulated with LPS and/or YL-109 for 4 hours. The H9c2 cells were stained with antibodies against cardiac troponin I (cTnI, red) and NF-$\kappa$B (green). Complete nuclei were stained with DAPI (blue). Scale bar = 50 $\mu$m. H-I, TNF-$\alpha$ (H), and IL-6 (I) levels in the supernatants of CHIP-knockdown H9c2 cells stimulated with LPS and/or YL-109 for 24 hours. Data are presented as mean ± SEM. $n = 5$; $^*P < 0.05$, $^{**}P < 0.01$. (For interpretation of the references to color in this figure legend, the reader is referred to the Web version of this article.)

$\kappa$B in the hearts of mice 4 hours after LPS injection (Fig 7, *E*). To further explore the therapeutic effect of YL-109 on cardiac dysfunction in septic mice, we examined the left ventricular function of mice 12 hours after LPS challenge via echocardiography. As shown in Fig 7, *F* and *G*, M-mode echocardiography evaluation demonstrated that LPS administration caused significant suppression of left ventricular contractile function in the mice, as evidenced by decreases in EF and FS compared with those measurements in the control mice. In contrast, administration of YL-109 markedly reversed the LPS-induced decrease in left ventricular EF and FS. To assess left ventricular diastolic function, the E/A ratio was calculated on the basis of Doppler-derived mitral inflow measurements. The results showed that LPS challenge significantly reduced the E/A ratio and that this effect was mitigated by treatment with YL-109 (Fig 7, *G*). These findings indicated that YL-109 protects against LPS-induced myocardial systolic and diastolic dysfunction. We further explored the effects of YL-109 on myocardial neutrophil infiltration and myeloperoxidase (MPO) levels by IHC analysis and Western blot. As shown in Fig 7, *H* and *I*, neutrophil infiltration and MPO levels in the hearts of mice were significantly increased after LPS stimulation for 4 hours. YL-109 treatment markedly attenuated LPS-induced increases in myocardial neutrophil infiltration and MPO levels.

To further verify the therapeutic effect of YL-109 on cardiac dysfunction in septic mice and determine whether this effect is limited to the LPS model, the CLP-induced polymicrobial sepsis mouse model was established and we subcutaneously injected YL-109 at a dose of 10 mg/kg 2 hours after CLP treatment. Twenty hours post-CLP surgery, the septic mice showed marked decrease in left ventricular EF and FS and the E/A ratio, and these alterations were significantly reversed by 10 mg/kg YL-109 treatment (Fig 8, *A* and *B*). YL-109 also alleviated the elevations in neutrophil infiltration and MPO expression in the hearts of mice 20 hours after CLP surgery (Fig 8, *C* and *D*). Moreover, as shown in Fig 8, *E* and *F*, cardiac TNF-$\alpha$ and IL-6 contents were markedly increased

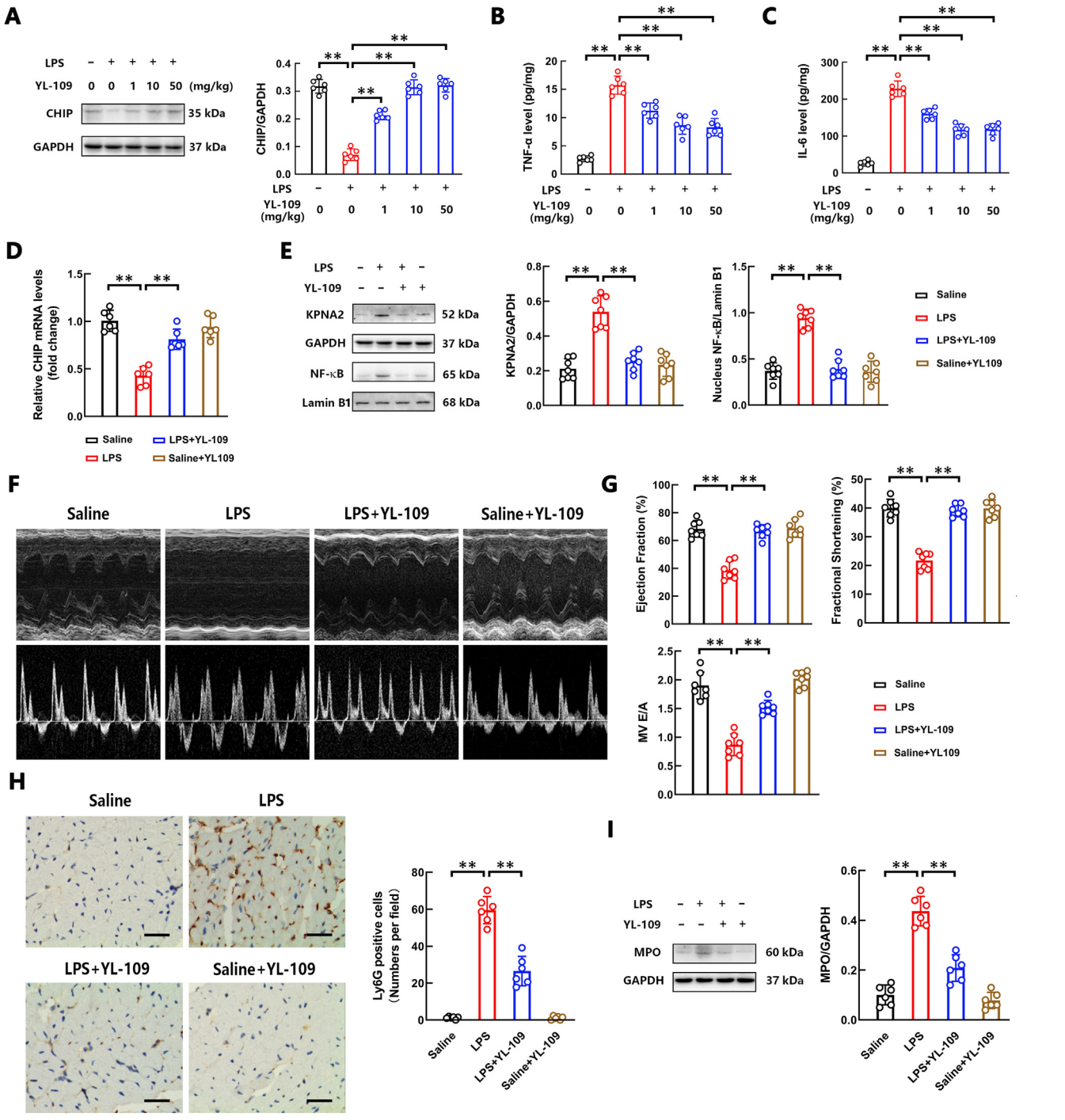


**Fig 7.** YL-109 prevented LPS-induced cardiac dysfunction by upregulating cardiac CHIP expression. (A) The protein expression of CHIP in the hearts of mice after LPS and different doses of YL-109 stimulation. (B and C) TNF-$\alpha$ (B) and IL-6 (C) levels in the myocardium of LPS-stimulated mice treated with different doses of YL-109. (D) The mRNA expression of CHIP in the hearts of mice after LPS treatment with or without 10 mg/kg YL-109. (E) The cardiac levels of KPNA2 and nuclear NF-$\kappa$B in mice challenged with LPS and/or YL-109. Quantifications of the relative protein levels are shown on the right-hand side of the images. (F) Representative M-mode and Doppler wave mode echocardiograms of mice treated with LPS and/or YL-109. (G) Quantitative group data obtained from the echocardiographic measurements: ejection fraction, fractional shortening and mitral valve E/A ratio (MV E/A). (H) Representative IHC images showing Ly6G level in the heart tissues of mice treated with LPS and/or YL-109 (left). Scale bar = 100 $\mu$m. The numbers of Ly6G-positive cells per field were calculated based on 5 randomly selected fields of stained cardiac tissues (right). (I) The level of cardiac MPO in mice challenged with LPS and/or YL-109. Quantification of the relative MPO level is shown on the right-hand side of the images. Data are presented as mean ± SEM. $n = 6$ or 7; $^{*}P < 0.05$, $^{**}P < 0.01$. (For interpretation of the references to color in this figure legend, the reader is referred to the Web version of this article.)

in the mice 20 hours after CLP challenge compared to those in the control. YL-109 significantly decreased the levels of cardiac TNF-$\alpha$ and IL-6 in CLP-stimulated mice. The myocardial CHIP mRNA and protein expression levels in septic mice treated with YL-109 were significantly higher than those in the CLP model group 12 hours after CLP surgery (Fig 8, *G* and *H*). Septic mice displayed markedly elevated levels of KPNA2 and nuclear NF-$\kappa$B in the left ventricular myocardium 12 hours after CLP surgery, and these levels were decreased by YL-109 treatment (Fig 8, *H*). In accordance with the previous results of this study, these data demonstrated that YL-109 ameliorates septic cardiac dysfunction

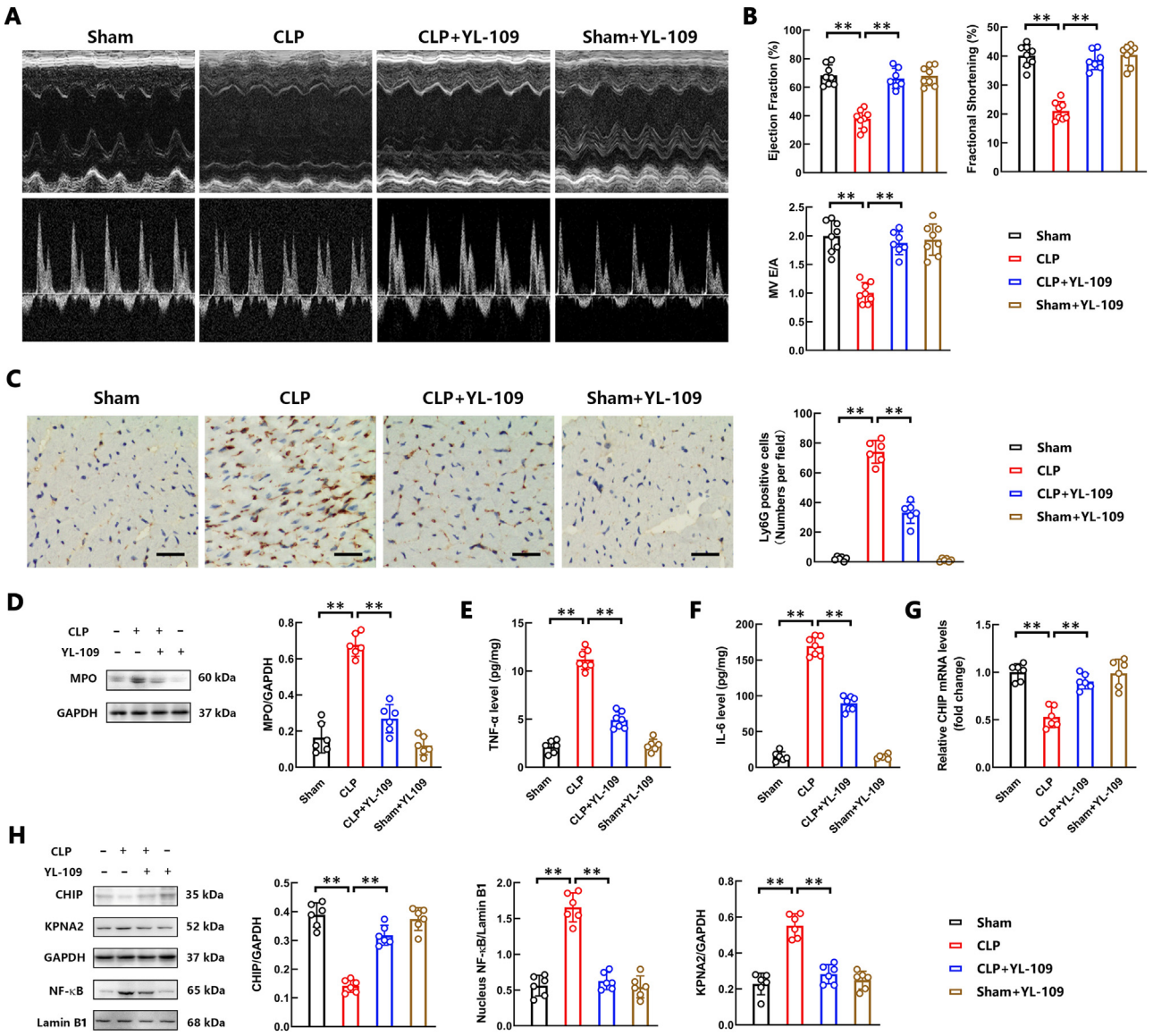


**Fig 8.** YL-109 alleviated cardiac dysfunction in mice subjected to CLP. (A) Representative M-mode and Doppler wave mode echocardiograms of mice treated with CLP and/or YL-109. (B) Quantitative group data obtained from echocardiographic measurements: ejection fraction, fractional shortening and mitral valve E/A ratio (MV E/A). (C) Representative IHC images showing Ly6G level in the heart tissues of mice treated with CLP and/or YL-109 (left). Scale bar = 100 $\mu$m. The numbers of Ly6G-positive cells per field were calculated based on 5 randomly selected fields of stained cardiac tissues (right). (I) The level of cardiac MPO in mice challenged with CLP and/or YL-109. Quantification of the relative MPO level is shown on the right-hand side of the images. E-F, TNF-$\alpha$ (E), and IL-6 (F) levels in the myocardium of mice after CLP and/or YL-109 stimulation. (G) The mRNA expression of CHIP in the hearts of mice with CLP and/or YL-109 treatment. (H) The cardiac levels of CHIP, KPNA2, and nuclear NF-$\kappa$B in CLP and/or YL-109-challenged mice. Quantifications of the relative protein levels are shown on the right-hand side of the images. Data are presented as mean ± SEM. $n = 6–8$; $^*P < 0.05$, $^{**}P < 0.01$. (For interpretation of the references to color in this figure legend, the reader is referred to the Web version of this article.)

by upregulating CHIP expression, which suppresses KPNA2 expression, NF-$\kappa$B activation, and proinflammatory cytokine release.

## Discussion

CHIP, functioning as both an E3 ligase and cochaperone, is ubiquitously expressed in a variety of tissues and cells, especially in hypermetabolic tissues such as cardiac and skeletal muscle.[11,12] Studies have widely explored the cardiac protective effect of CHIP against ischemic injury and other stress stimuli.[13-16] However, its potential role in sepsis-induced cardiac dysfunction and the underlying mechanisms have not been fully elucidated. Here we report several novel and important findings regarding the role of CHIP in cardiac dysfunction initiated by sepsis: (1) CHIP protein and mRNA levels were reduced in the myocardium of the mouse sepsis model; (2) c-Jun directly suppressed the transcription of CHIP in cardiomyocytes; (3) CHIP regulated KPNA2 stability via promoted its proteasomal degradation; (4) upregulation of KPNA2 promoted the transport of NF-$\kappa$B into the nucleus, resulting in TNF-$\alpha$ and IL-6 production in cardiomyocytes after LPS stimulation; (5) cardiac-specific overexpression of CHIP reduced inflammation in the cardiac tissue and inhibited cardiac dysfunction in the septic mice; and (6) the therapeutic effect of YL-109 on cardiac dysfunction depended on the upregulation of CHIP expression.

The construction of a septic model is a necessary prerequisite for laboratory research on sepsis. Two methods, CLP and peritoneal injection of LPS, are commonly used to establish sepsis models.[33] The sepsis model established by injection of LPS shows a rapid inflammatory response, and in a short period of time, experimental animals release

high levels of inflammatory cytokines. Moreover, this model is easy to establish, enabling study reproducibility.[34] However, LPS model cannot fully recapitulate the clinical features of patients with sepsis.[35] The CLP model shows better clinical relevance through simulating sepsis caused by peritoneal infection.[36] In this research, we used both methods to establish mouse models of sepsis for animal study. We first demonstrated that CHIP protein and mRNA levels were downregulated in a time-dependent fashion in the myocardium of the septic mice. Moreover, we found that LPS inhibited CHIP expression of cardiomyocytes in a dose-dependent manner *in vitro*. The transcription factors c-Jun/c-Fos and NF-$\kappa$B activated by LPS regulate target proteins such as TNF-$\alpha$ and IL-6 by interacting with their promoter regions.[37] Considering that transcription factors can negatively regulate target genes by binding to promoter regulatory sequences,[38,39] we hypothesized that c-Jun/c-Fos and NF-$\kappa$B not only promote the release of cytokines but also suppress the expression of CHIP at the transcriptional level. Our study showed that only the c-Jun/c-Fos inhibitor SP600125 reversed CHIP protein and mRNA expression in cardiomyocytes after LPS treatment, whereas the NF-$\kappa$B inhibitor exerted no effect on that. Thus, CHIP may be a downstream target of c-Jun/c-Fos in cardiomyocytes stimulated by LPS. We further confirmed that c-Jun but not c-Fos significantly altered CHIP expression by affecting the promoter regulatory region of the *stub1* gene. This finding supported the idea that LPS-initiated c-Jun activation and translocation into the nucleus are the main causes of downregulated CHIP expression in the myocardium of mice with sepsis.

Through the C-terminal U-box domain, CHIP interacts with its target proteins to transfer ubiquitin from an E2-conjugating enzyme.[40] In a recent study, we constructed a novel approach termed "orthogonal ubiquitin transfer (OUT)" to profile CHIP substrate specificity and found that KPNB1, a member of the karyopherin superfamily, appeared on the list of CHIP potential targets.[23] This finding implied that another superfamily member, KPNA2, may be a direct target for CHIP ubiquitination. We confirmed this hypothesis by *in vitro* experiments. Downregulation of CHIP in H9c2 cardiac cells significantly reduced the polyubiquitination and degradation of KPNA2. Moreover, overexpression of CHIP accelerated the proteasomal degradation of KPNA2. Karyopherin proteins are involved in the nucleocytoplasmic trafficking of cargo proteins and certain RNA across the nuclear pore complex into and out of the cell nucleus.[41] Studies have demonstrated that, as an adaptor protein, KPNA2 plays a key role in multiple biological functions by mediating the nuclear translocation of target proteins via the nuclear pore complex.[42,43] NF-$\kappa$B is retained in the cytoplasm until it is activated in response to stimulation. Prior research has shown that nuclear import of NF-$\kappa$B in several types of cells is regulated by KPNA2, which first binds to the NF-$\kappa$B protein and subsequently recruits importin $\beta$.[21,22] Given the pivotal role of the NF-$\kappa$B signaling pathway in inflammation, we next focused on the possible association between KPNA2 and NF-$\kappa$B subcellular translocation in H9c2 cardiac cells in the case of LPS stimulation. Following LPS stimulation, KPNA2 expression was obviously upregulated, and immunoprecipitation revealed an interaction between KPNA2 and NF-$\kappa$B in H9c2 cells. We confirmed that inhibiting KPNA2 expression with siRNA greatly attenuated LPS-induced translocation of NF-$\kappa$B from the cytoplasm to the nucleus in H9c2 cells. More importantly, knockdown of KPNA2 decreased the release of TNF-$\alpha$ and IL-6 from H9c2 cells 24 hours after LPS stimulation. Further study demonstrated that CHIP overexpression markedly induced the degradation of KPNA2, thereby inhibiting NF-$\kappa$B nuclear import that decreased the production of TNF-$\alpha$ and IL-6 in LPS-treated H9c2 cells. Conversely, knockdown of CHIP markedly promoted LPS-induced NF-$\kappa$B nuclear import. I$\kappa$B$\alpha$ phosphorylation is a key event for the activation of NF-$\kappa$B. Under normal conditions, NF-$\kappa$B is sequestered in cytoplasm by I$\kappa$B$\alpha$. Following the activation of related signaling pathways, the phosphorylation and degradation of I$\kappa$B$\alpha$ are initiated, which causes the release of NF-$\kappa$B. Then, NF-$\kappa$B is translocated into the nucleus, where it promotes target gene expression.[44] In this study, overexpression of CHIP did not affect either the cellular NF-$\kappa$B elevation or I$\kappa$B$\alpha$ phosphorylation induced by LPS in cardiomyocytes, which confirmed the hypothesis that CHIP functions by disrupting the transportation of NF-$\kappa$B from the cytoplasm to the nucleus rather than by reducing NF-$\kappa$B level or inhibiting the upstream signaling pathway of NF-$\kappa$B. The activity of CHIP is initiated through interaction with Hsp70, subsequently promoting protein degradation by polyubiquitination.[45] Studies have reported that LPS upregulates the expression of Hsp70 in cardiac myocytes.[46,47] Therefore, given the increase of Hsp70 caused by LPS, CHIP may play an enhanced role in promoting the degradation of excessive KPNA2 in LPS-stimulated cardiomyocytes. Thus, upregulation of CHIP against LPS initiated the inflammatory processes of cardiomyocytes through promoting KPNA2 ubiquitination and degradation, which inhibited NF-$\kappa$B nuclear import.

Cardiac dysfunction is a common complication associated with increased mortality in septic patients.[48,49] Numerous studies have demonstrated that inflammatory cytokines, including TNF-$\alpha$ and IL-6, initiated by pathogen-associated molecular patterns, such as LPS, are key factors in myocardial injury during sepsis.[50,51] Therefore, finding a target for inhibiting the inflammatory response and thus improve cardiac function for the treatment of septic cardiac dysfunction is clearly important. Based on the results of *in vitro* experiments, CHIP overexpression can inhibit the LPS-induced release of TNF-$\alpha$ and IL-6 from cardiomyocytes. Consistently, using transgenic mouse models constitutively overexpressing CHIP in the heart, we further demonstrated that myocardial overexpression of CHIP exerted an effect on improving cardiac function and survival in septic mice. Our present results also showed that the sepsis-induced production of proinflammatory cytokines such as TNF-$\alpha$ and IL-6 was markedly suppressed in CHIP OE mice and this effect was associated with the inactivation of NF-$\kappa$B via inhibited KPNA2 expression. These results suggest that CHIP is an important target for improving cardiac function and the agents that upregulate CHIP expression may play a role in ameliorating cardiac dysfunction during sepsis. The compound YL-109 has been reported to induce CHIP expression in breast cancer cells.[32] In this study, we demonstrated that YL-109 significantly restored both the mRNA and protein levels of CHIP in LPS-treated neonatal rat cardiomyocytes. Moreover, YL-109 inhibited LPS-induced upregulation of KPNA2 and NF-$\kappa$B activation as well as TNF-$\alpha$ and IL-6 release from cardiomyocytes. We found that the effect of YL-109 on suppressing inflammation triggered by LPS was CHIP dependent in cardiomyocytes. Subsequently, the therapeutic effect of YL1-09 on cardiac dysfunction was confirmed by using 2 sepsis mouse models that were established by CLP surgery and intraperitoneal LPS injection. The administration of YL-109 increased cardiac CHIP expression and improved both the cardiac systolic and diastolic functions in the septic mice. Moreover, YL-109 reduced cardiac KPNA2 expression and activation of NF-$\kappa$B, resulting in inhibition of neutrophil infiltration and proinflammatory cytokines production in the myocardium of mice with sepsis. Thus, CHIP upregulation mediated the reduction in inflammatory response by inhibiting the KPNA2/NF-$\kappa$B axis, explaining the cardioprotective effect of YL-109 during sepsis. Given its distinct role in cardioprotection, YL-109 may be a promising clinical therapeutic agent for patients with septic cardiomyopathy.

Our study has some limitations. First, the activation of c-Jun induced by LPS inhibits the transcription of CHIP in cardiomyocytes. As a transcription factor, c-Jun is difficult to directly cause protein degradation. Therefore, during sepsis, it is possible that c-Jun-mediated expression of other target genes may directly promote CHIP degradation in other ways. Second, based on our study and previous findings, the role of YL-109 in upregulation of CHIP expression is not cell-specific. The expression of CHIP in heart is significantly higher than that in other tissues and cells, which is the main reason for our attention to the effect of YL-109 on myocardium. However, YL-109 may also act on other tissues or inflammatory cells in sepsis. Third, we only studied the function of YL-109 in reversing cardiac CHIP expression of septic mice, and the mechanisms need to be studied in depth. This will help to explore distinct roles of YL-109 in sepsis.

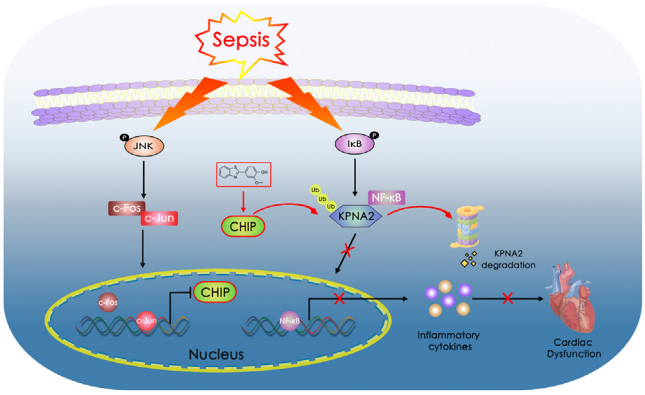


**Fig 9.** Schematic representation of signaling pathway mediating the downregulation of CHIP expression in septic myocardium and the mechanisms of CHIP-mediated improvement in cardiac dysfunction during sepsis. Sepsis induces the activation of c-Jun, which exerts an inhibitory action on CHIP transcription. CHIP can accelerate the ubiquitin-proteasome-mediated degradation of KPNA2, which suppresses sepsis-induced translocation of NF-κB from the cytoplasm to the nucleus, attenuating the release of proinflammatory cytokines and contributing cardiac function protection. (For interpretation of the references to color in this figure legend, the reader is referred to the Web version of this article.)

In conclusion, in this report, we provide the first evidence showing that LPS initiated the activation of c-Jun, which inhibited the transcription of CHIP in cardiomyocytes. More importantly, CHIP directly promoted proteasomal degradation of KPNA2, which suppressed sepsis-induced nuclear translocation of NF-κB in myocardium and then reduced TNF-α and IL-6 release, preventing cardiac dysfunction in septic mice (Fig 9). Therefore, we conclude that restoring CHIP expression in the heart protects against sepsis-triggered cardiac dysfunction, revealing a potential therapeutic role of CHIP in septic patients with cardiac dysfunction.

## Data Availability Statement

The authors declare that the data supporting the findings of this study are included in the article/Supplemental Material. Further inquiries can be directed to the corresponding authors.

## Ethics Statement

The animals used in this study were handled in strict accordance with the recommendations in the Guide for the Care and Use of Laboratory Animals of the National Institutes of Health. All animal procedures were reviewed and approved by the Animal Ethics Committee of Jinan University (Approval No. IACUC-20220531-01).

## Acknowledgments

Conflict of Interest: All authors have read the journal's policy on conflicts of interest and report no disclosed potential conflicts of interest related to this work.

This research was supported by the National Natural Science Foundation of China (Grant No. 82072138). All authors have read the journal's authorship agreement and that the manuscript has been reviewed by and approved by all named authors.

Author contributions are as follow: J. Liao, X. Y. Su, and M. Wang: Data curation, Formal analysis, Methodology, and Writing-original draft; L. C. Jang and X. Chen: Methodology; Z. X. Liu and G. Q. Tang: Data curation and Software; L. Zhou, H. M. Li and X. X. Lv: Formal analysis; J. Yin: Conceptualization and Resources; H. D. Wang: Project administration and Supervision; Y. Y. Wang: Project administration, Resources, Validation, Supervision, and Writing-review & editing. All authors have read and agreed to the published version of the manuscript.

We thank all members of the laboratory for their kindness and help.

## Supplementary materials

Supplementary material associated with this article can be found, in the online version, at doi:10.1016/j.trsl.2022.11.006.

## References

1. Singer M, Deutschman CS, Seymour CW, et al. The Third International Consensus definitions for sepsis and septic shock (Sepsis-3). JAMA 2016;315:801–10.
2. Jayaprakash N, Gajic O, Frank RD, Smischney N. Elevated modified shock index in early sepsis is associated with myocardial dysfunction and mortality. J Crit Care 2018;43:30–5.
3. Merx MW, Weber C. Sepsis and the heart. Circulation 2007;116:793–802.
4. Walley KR. Sepsis-induced myocardial dysfunction. Curr Opin Crit Care 2018;24:292–9.
5. Schumacher SM, Naga Prasad SV. Tumor necrosis factor-α in heart failure: an updated review. Curr Cardiol Rep 2018;20:117.
6. Jiang T, Peng D, Shi W, et al. IL-6/STAT3 signaling promotes cardiac dysfunction by upregulating FUNDC1-dependent mitochondria-associated endoplasmic reticulum membranes formation in sepsis mice. Front Cardiovasc Med 2021;8:790612.
7. Wang R, Xu Y, Fang Y, et al. Pathogenetic mechanisms of septic cardiomyopathy. J Cell Physiol 2022;237:49–58.
8. Murata S, Chiba T, Tanaka K. CHIP: a quality-control E3 ligase collaborating with molecular chaperones. Int J Biochem Cell Biol 2003;35:572–8.
9. Ballinger CA, Connell P, Wu Y, et al. Identification of CHIP, a novel tetratricopeptide repeat-containing protein that interacts with heat shock proteins and negatively regulates chaperone functions. Mol Cell Biol 1999;19:4535–45.
10. Connell P, Ballinger CA, Jiang J, et al. The co-chaperone CHIP regulates protein triage decisions mediated by heat-shock proteins. Nat Cell Biol 2001;3:93–6.
11. Ranek MJ, Stachowski MJ, Kirk JA, Willis MS. The role of heat shock proteins and co-chaperones in heart failure. Philos Trans R Soc Lond B Biol Sci 2018;373:20160530.
12. Wang T, Wang W, Wang Q, et al. The E3 ubiquitin ligase CHIP in normal cell function and in disease conditions. Ann N Y Acad Sci 2020;1460:3–10.
13. Zhang C, Xu Z, He XR, et al. CHIP, a cochaperone/ubiquitin ligase that regulates protein quality control, is required for maximal cardioprotection after myocardial infarction in mice. Am J Physiol Heart Circ Physiol 2005;288:H2836–42.
14. Ranek MJ, Oeing C, Sanchez-Hodge R, et al. CHIP phosphorylation by protein kinase G enhances protein quality control and attenuates cardiac ischemic injury. Nat Commun 2020;11:5237.
15. Ali A, Kuo WW, Kuo CH, et al. E3 ligase activity of carboxyl terminus of Hsc70 interacting protein (CHIP) in Wharton's jelly derived mesenchymal stem cells improves their persistence under hyperglycemic stress and promotes the prophylactic effects against diabetic cardiac damages. Bioeng Transl Med 2021;6:e10234.
16. Wang L, Zhang TP, Zhang Y, et al. Protection against doxorubicin-induced myocardial dysfunction in mice by cardiac-specific expression of carboxyl terminus of hsp70-interacting protein. Sci Rep 2016;6:28399.
17. Mosammaparast N, Pemberton LF. Karyopherins: from nuclear-transport mediators to nuclear-function regulators. Trends Cell Biol 2004;14:547–56.
18. Fried H, Kutay U. Nucleocytoplasmic transport: taking an inventory. Cell Mol Life Sci 2003;60:1659–88.
19. Lange A, Mills RE, Lange CJ, et al. Classical nuclear localization signals: definition, function, and interaction with importin alpha. J Biol Chem 2007;282:5101–5.
20. Pumroy RA, Cingolani G. Diversification of importin-α isoforms in cellular trafficking and disease states. Biochem J 2015;466:13–28.
21. Liang P, Zhang H, Wang G, et al. KPNB1, XPO7 and IPO8 mediate the translocation ofNF-κB/p65 into the nucleus. Traffic 2013;14:1132–43.
22. Cai Y, Shen Y, Gao L, et al. Karyopherin alpha 2 promotes the inflammatory response in rat pancreatic acinar cells via facilitating NF-κB activation. Dig Dis Sci 2016;61:747–57.
23. Bhuripanyo K, Wang Y, Liu X, et al. Identifying the substrate proteins of U-box E3s E4B and CHIP by orthogonal ubiquitin transfer. Sci Adv 2018;4:e1701393.
24. Yu X, Wang Y, Yang D, et al. α(2A)-adrenergic blockade attenuates septic cardiomyopathy by increasing cardiac norepinephrine concentration and inhibiting cardiac endothelial activation. Sci Rep 2018;8:5478.
25. Jiang L, Li D, Wang C, et al. Decreased expression of karyopherin-α 1 is related to the malignant degree of cervical cancer and is critical for the proliferation of Hela cells. Pathol Oncol Res 2022;28:1610518.
26. Yang D, Dai X, Xing Y, et al. Intrinsic cardiac adrenergic cells contribute to LPS-induced myocardial dysfunction. Commun Biol 2022;5:96.
27. Wang Y, Wang Y, Yang D, et al. β-Adrenoceptor stimulation promotes LPS-induced cardiomyocyte apoptosis through activating PKA and enhancing CaMKII and IκBα phosphorylation. Crit Care 2015;19:76.
28. Liu X, Zhao B, Sun L, et al. Orthogonal ubiquitin transfer identifies ubiquitination substrates under differential control by the two ubiquitin activating enzymes. Nat Commun 2017;8:14286.
29. Kim SY, Hassan AHE, Chung KS, et al. Mosloflavone-resveratrol hybrid TMS-HDMF-5z exhibits potent in vitro and in vivo anti-inflammatory effects through NF-κB, AP-1, and JAK/STAT inactivation. Front Pharmacol 2022;13:857789.
30. Yao C, Purwanti N, Karabasil MR, et al. Potential down-regulation of salivary gland AQP5 by LPS via cross-coupling of NF-kappaB and p-c-Jun/c-Fos. Am J Pathol 2010;177:724–34.
31. Korbecki J, Bajdak-Rusinek K. The effect of palmitic acid on inflammatory response in macrophages: an overview of molecular mechanisms. Inflamm Res 2019;68:915–32.

32. Hiyoshi H, Goto N, Tsuchiya M, et al. 2-(4-Hydroxy-3-methoxyphenyl)-benzothiazole suppresses tumor progression and metastatic potential of breast cancer cells by inducing ubiquitin ligase CHIP. Sci Rep 2014;4:7095.
33. Hahmeyer M, da Silva-Santos JE. Rho-proteins and downstream pathways as potential targets in sepsis and septic shock: what have we learned from basic research. Cells 2021;10:1844.
34. Dickson K, Lehmann C. Inflammatory response to different toxins in experimental sepsis models. Int J Mol Sci 2019;20:4341.
35. Osuchowski MF, Ayala A, Bahrami S, et al. Minimum quality threshold in pre-clinical sepsis studies (MQTiPSS): an international expert consensus initiative for improvement of animal modeling in sepsis. Infection 2018;46:687–91.
36. Hubbard WJ, Choudhry M, Schwacha MG, et al. Cecal ligation and puncture. Shock 2005;24(suppl 1):52–7.
37. Facchin BM, Dos Reis GO, Vieira GN, et al. Inflammatory biomarkers on an LPS-induced RAW 264.7 cell model: a systematic review and meta-analysis. Inflamm Res 2022;71:741–58.
38. Velthuijs N, Meldal B, Geessinck Q, et al. Integration of transcription coregulator complexes with sequence-specific DNA-binding factor interactomes. Biochim Biophys Acta Gene Regul Mech 2021;1864:194749.
39. Shaulian E, Karin M. AP-1 as a regulator of cell life and death. Nat Cell Biol 2002;4:E131–6.
40. McDonough H, Patterson C. CHIP: a link between the chaperone and proteasome systems. Cell Stress Chaperones 2003;8:303–8.
41. Wing CE, Fung HYJ, Chook YM. Karyopherin-mediated nucleocytoplasmic transport. Nat Rev Mol Cell Biol 2022;23:307–28.
42. Han Y, Wang X. The emerging roles of KPNA2 in cancer. Life Sci 2020;241:117140.
43. Tseng SF, Chang CY, Wu KJ, Teng SC. Importin KPNA2 is required for proper nuclear localization and multiple functions of NBS1. J Biol Chem 2005;280:39594–600.
44. Hu Y, O'Boyle K, Auer J, et al. Multiple UBXN family members inhibit retrovirus and lentivirus production and canonical NFκB signaling by stabilizing IκBα. PLoS Pathog 2017;13:e1006187.
45. Seo J, Han SY, Seong D, Han HJ, Song J. Multifaceted C-terminus of HSP70-interacting protein regulates tumorigenesis via protein quality control. Arch Pharm Res 2019;42:63–75.
46. Löw-Friedrich I, Weisensee D, Mitrou P, Schoeppe W. Cytokines induce stress protein formation in cultured cardiac myocytes. Basic Res Cardiol 1992;87:12–8.
47. Meng X, Brown JM, Ao L, et al. Endotoxin induces cardiac HSP70 and resistance to endotoxemic myocardial depression in rats. Am J Physiol 1996;271:C1316–24.
48. Martin L, Derwall M, Al Zoubi S, et al. The septic heart: current understanding of molecular mechanisms and clinical implications. Chest 2019;155:427–37.
49. Fenton KE, Parker MM. Cardiac function and dysfunction in sepsis. Clin Chest Med 2016;37:289–98.
50. L'Heureux M, Sternberg M, Brath L, et al. Sepsis-induced cardiomyopathy: a comprehensive review. Curr Cardiol Rep 2020;22:35.
51. Beesley SJ, Weber G, Sarge T, et al. Septic cardiomyopathy. Crit Care Med 2018;46:625–34.